A Ground-Based Study on Extruder Standoff Distance for the 3D Printing in Zero Gravity Technology Demonstration Mission

T.J. Prater, Q.A. Bean, N.J. Werkheiser, R.D. Beshears, T.D. Rolin, E.M. Rabenberg, and H.A. Soohoo
Marshall Space Flight Center, Huntsville, Alabama

F.E. Ledbetter III
Wheelhouse Consulting, LLC
Marshall Space Flight Center, Huntsville, Alabama

S.C. Bell
Jacobs Engineering
Marshall Space Flight Center, Huntsville, Alabama

The NASA STI Program…in Profile

Since its founding, NASA has been dedicated to the advancement of aeronautics and space science. The NASA Scientific and Technical Information (STI) Program Office plays a key part in helping NASA maintain this important role.

The NASA STI Program Office is operated by Langley Research Center, the lead center for NASA's scientific and technical information. The NASA STI Program Office provides access to the NASA STI Database, the largest collection of aeronautical and space science STI in the world. The Program Office is also NASA's institutional mechanism for disseminating the results of its research and development activities. These results are published by NASA in the NASA STI Report Series, which includes the following report types:

- TECHNICAL PUBLICATION. Reports of completed research or a major significant phase of research that present the results of NASA programs and include extensive data or theoretical analysis. Includes compilations of significant scientific and technical data and information deemed to be of continuing reference value. NASA's counterpart of peer-reviewed formal professional papers but has less stringent limitations on manuscript length and extent of graphic presentations.

- TECHNICAL MEMORANDUM. Scientific and technical findings that are preliminary or of specialized interest, e.g., quick release reports, working papers, and bibliographies that contain minimal annotation. Does not contain extensive analysis.

- CONTRACTOR REPORT. Scientific and technical findings by NASA-sponsored contractors and grantees.

- CONFERENCE PUBLICATION. Collected papers from scientific and technical conferences, symposia, seminars, or other meetings sponsored or cosponsored by NASA.

- SPECIAL PUBLICATION. Scientific, technical, or historical information from NASA programs, projects, and mission, often concerned with subjects having substantial public interest.

- TECHNICAL TRANSLATION. English-language translations of foreign scientific and technical material pertinent to NASA's mission.

Specialized services that complement the STI Program Office's diverse offerings include creating custom thesauri, building customized databases, organizing and publishing research results…even providing videos.

For more information about the NASA STI Program Office, see the following:

- Access the NASA STI program home page at <http://www.sti.nasa.gov>

- E-mail your question via the Internet to <help@sti.nasa.gov>

- Phone the NASA STI Help Desk at 757–864–9658

- Write to:
  NASA STI Information Desk
  Mail Stop 148
  NASA Langley Research Center
  Hampton, VA 23681–2199, USA

A Ground-Based Study on Extruder Standoff Distance for the 3D Printing in Zero Gravity Technology Demonstration Mission

T.J. Prater, Q.A. Bean, N.J. Werkheiser, R.D. Beshears, T.D. Rolin, E.M. Rabenberg, and H.A. Soohoo
Marshall Space Flight Center, Huntsville, Alabama

F.E. Ledbetter III
Wheelhouse Consulting, LLC
Marshall Space Flight Center, Huntsville, Alabama

S.C. Bell
Jacobs Engineering
Marshall Space Flight Center, Huntsville, Alabama

TABLE OF CONTENTS

TABLE OF CONTENTS (Continued)

LIST OF FIGURES

LIST OF FIGURES (Continued)

LIST OF TABLES

LIST OF ACRONYMS

3DP	3D print
ABS	acrylonitrile butadiene styrene
AM	additive manufacturing
ASTM	American Society of Materials Testing
BSE	backscatter electron
CAD	computer-aided design
CT	computed tomography
ETU	engineering test unit
FDM	fused deposition modeling
FOD	foreign object debris
FTIR	Fourier transform infrared spectroscopy
HDI	high density inclusion
ISM	in-space manufacturing
ISS	International Space Station
LDI	low density indication
LED	light-emitting diode
MSFC	Marshall Space Flight Center
SEM	scanning electron microscopy
TP	Technical Publication
UTS	ultimate tensile strength
zero G	zero gravity

TECHNICAL PUBLICATION

A GROUND-BASED STUDY ON EXTRUDER STANDOFF DISTANCE FOR THE 3D PRINTING IN ZERO GRAVITY TECHNOLOGY DEMONSTRATION MISSION

1. PURPOSE AND SCOPE OF STUDY

In 2014, NASA, in cooperation with Made in Space, Inc., launched a 3D printer to the International Space Station (ISS) with the goal of demonstrating the technology for space applications and evaluating the effect of microgravity on the fused deposition modeling (FDM) process. Manufacturing technologies, such as FDM, could ultimately find use on long duration, long endurance missions where cargo resupply is not readily available. In-space manufacturing (ISM) has the potential to reduce logistics requirements and enhance crew safety by enabling a rapid response capability.[1]

As part of phase I operations, ground specimens printed with the flight printer prior to its launch to the ISS, were compared against specimens of identical geometry built on ISS from November to December 2014. This first phase of prints from the mission were evaluated at NASA Marshall Space Flight Center (MSFC) from April 2015 to March 2016, where specimens underwent mass measurement, structured light scanning, x-ray/computed tomography (CT), mechanical testing, scanning electron microscopy (SEM), and Fourier transform infrared spectroscopy (FTIR). Results of testing from the phase I specimens are summarized in references 2 and 3.

Some differences in mechanical properties and specimen structure between ground specimens and analogous flight specimens were observed. Potential explanations for the discrepancy (microgravity effects, differences in manufacturing process settings between ground and flight printer operations, and aging of the filament feedstock) were considered and follow-on studies were developed to pinpoint the sources of variability between the ground and flight data set.[2] FTIR analysis was unable to detect significant chemical differences between the ground and flight printed specimens—flight feedstock was 6 months older than ground feedstock at the time of printing—and largely ruled out any aging effects on material performance. SEM analysis of representative material cross sections failed to show differences in filament slump between specimen classes and was, in general, not indicative of an obvious microgravity effect on internal material structure.[3] However, comparative SEM analysis noted greater material buildup at the base of the flight tensile specimens and dramatic differences in fiber structure between the ground and flight specimens that suggest differences in the way the ground and flight specimens were manufactured. The purpose of the study detailed here is to provide a better understanding of the sources of variability in the phase I specimens using the engineering test unit, a ground-based unit identical to the flight printer from the 3D print (3DP) technology demonstration mission.

One known source of process variability in the 3DP phase I data set stems from differences in the calibration setting for the printer during flight and ground prints. The *z*-calibration value, which determines the distance of the extruder head from the build tray the extruded material is deposited on, was adjusted based on visual feedback during phase I on-orbit operations of the 3DP unit. This value was held constant for the ground-based prints. Figure 1 illustrates the relationship between the *z*-calibration value (commanded by the user prior to printing) and the extruder standoff distance (the distance from the tip of the extruder to the build tray). The *z*-calibration distance for the ground-manufactured 3DP specimens was held constant at 2.2 mm. For flight prints, this tip to tray distance—also referred to as the extruder standoff distance—is not directly measurable since the printer does not have closed-loop positional feedback. The commanded value for the flight prints ranged from 2.39 mm to 2.84 mm. No two prints had the same process setting.

Extruder Tip (0.4 mm Orifice)

Nominal tip to tray distance for 0.4 mm extruder tip is about 0.2 mm

Tip to Tray Distance

z-Calibration Distance

Build Plate Build Position

Build Plate Home Position
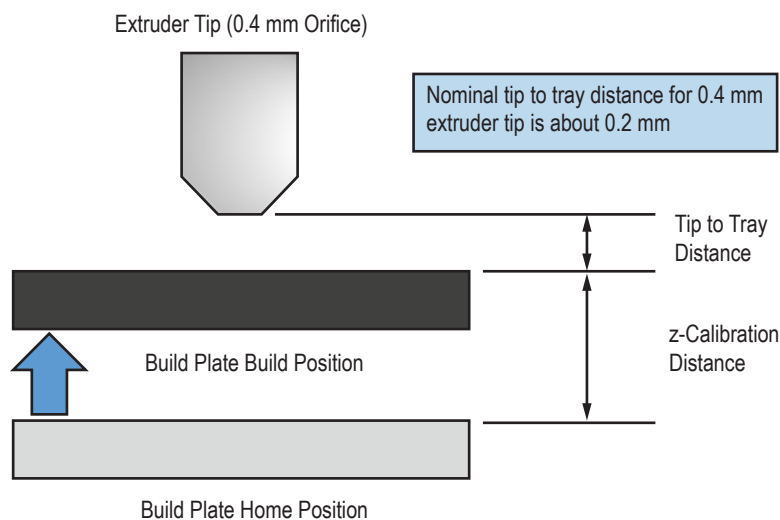
Figure 1. Illustration of relationship between *z*-calibration and tip to tray distance.

Based on data from structured light scanning and corroborated by SEM analysis, the extruder tip was positioned too close to the tray during flight prints, resulting in specimens with protrusions along the geometric boundaries. Per Rodriguez et al., protrusions suggest an off-nominal extruder standoff distance.[4] The discrepancy in this machine setting for ground and flight specimens may explain why flight specimens were generally denser than their ground counterparts, a key finding documented in references 2 and 3. The tip to tray distance hypothesis developed based on the 3DP phase I data set postulates that the closer position of the extruder tip to the specimen during flight prints (and variation of this distance) potentially explains some of the measured variability in material properties for ground and flight specimens. While no consistent correlation was detected between the *z*-calibration value and density or mechanical properties for the flight prints, literature on manufacturing process optimization for FDM indicates that extruder standoff distance is a parameter that can influence thermal flow and cooling rate, deposition rate, and interlayer configuration. Variations in processing conditions are closely linked to variations in microstructure, which in turn influence mechanical performance of the resulting part.

Using the engineering test unit (ETU), the flight-like unit for 3DP, a matrix of tensile coupons, layer quality specimens, and compression coupons were printed at z-calibration values which broadly mimic the ground and flight operational settings of 3DP phase I. Table 1 summarizes the specimens and the systematic variation of the extruder standoff distance from its nominal position. Tensile coupons are a type IV geometry from ASTM D638,[5] and compression coupons are per ASTM D695.[6] The layer quality specimen is a square columnar specimen measuring 1.18 inch in height and 0.40 inch in length and width. All specimens are built at a ±45 layup pattern.

Table 1. Extruder standoff distance study build matrix.

Sample Type	Calibration Condition	Quantity
Tensile	Nominal	3
Compression		3
Layer quality		2
Tensile	–0.02 mm	3
Compression		3
Layer quality		2
Tensile	0.05 mm	3
Compression		3
Layer quality		2
Tensile	0.1 mm	3
Compression		3
Layer quality		2

Prints for which the build plate is moved in the downward direction—increasing the extruder standoff distance so that the part is built 'too far' from the extruder tip—have a calibration condition that is negatively biased. The –0.02 mm level selected corresponds to a position with the extruder tip 0.02 mm farther from the nominal/optimal condition. This distance represents the highest location of the extruder tip that will still yield a testable part. Prints for which the extruder is closer to the build tray are positively biased from the nominal condition. 0.05 mm corresponds to a condition where the build tray is translated upward by 0.05 mm. Similarly, the 0.1 mm level in the design of experiments indicates translation of the build tray 0.1 mm from its 'home' position. The matrix of specimens for the study is summarized in table 1. Flight feedstock from the same lot as the flight and ground prints from phase I operations was used for this study.

One nuance of the study parameters is that the nominal z-calibration values—from which the build tray is moved upward or downward in the indicated increments—were found to be specific to the geometry of the part. The optimal value for the tensile specimen was determined from iterative prints on the ETU to be 2.99. The compression specimen optimal setting was 2.97, and layer quality specimen was 3. It is important to note that the z-calibration values in the tip to tray experiments are not directly comparable to the z-calibration values for the flight and ground specimens for 3DP phase I. This is, in large part, because each print tray used for the ETU and flight unit has a slightly different topology. Print trays must be periodically replaced over the course of a series of

builds if significant part adhesion occurs, which leads to residual material accumulation on the tray. For example, four print tray changes took place during the printing of the 21 flight parts for 3DP phase I operations. Tray to tray surface variability and differences in the extruder are variables that will slightly change the z-calibration value. To compound these issues, z-calibration can also vary based on the location of the specimen on the print tray. The trays themselves are not flat and, in some instances, extruded material tends to fill the grooves of the tray, making it harder for the part to adhere and artificially decreasing the tip to tray distance. These issues are inherent limitations of the 3DP hardware and difficult to control without substantial modifications/upgrades to both the flight and ground units.

Given these limitations, the extruder standoff distance study is not intended to be a precise replicate of ground or flight operations of the 3DP unit, but an attempt to broadly recreate the ground (specimens built 'too far' from extruder tip) and flight (specimens built 'too close' to the extruder) conditions. The scope of the study was to optimize the extruder standoff distance for a particular geometry and then systematically vary this distance to determine the sensitivity of material outcomes to subtle adjustments in z-calibration. For the phase I flight prints, the extruder was moved a maximum of 0.4 mm during the course of operations.

In this Techncial Publication (TP), the flight and ground data from various phases of testing are often plotted along side data from the extruder standoff distance study for context, but differences in the processing conditions, which, in many cases, are not robustly quantifiable, should be considered when evaluating the data side by side. The extruder standoff distance study seeks to:

(1) Quantify the influence of minute changes in the position of the extruder tip relative to the build plate on structure and properties of materials produced under these specific conditions using the ETU.

(2) Determine whether relationships in (1) might be extrapolated to explain a process variation in the 3DP phase I data set.

Specimens from the study of extruder standoff distance underwent mass evaluation, x-ray/CT, structured light scanning, surface metrology (compression specimens only), mechanical testing (compression and tensile specimens), and microscopy (optical and SEM). Results of these evaluations are detailed in subsequent sections. Recall that while the z-calibration settings for the tip to tray specimens and those for the 3DP phase I flight and ground prints are not directly comparable due to variability in the topology of the print trays, manufacturing process settings for this work were selected to closely approximate the ground and flight conditions. The –0.02 mm condition closely approximates the ground prints from 3DP phase I (build with tray too far from the extruder) and the 0.1 mm and 0.05 mm conditions approximate the manufacturing process settings for the flight prints (build with tray too close to the extruder). Specimen data are compared within the ground and flight data sets for context where appropriate. Table 2 summarizes the phases of testing and number/type of specimens for each evaluation.

Table 2. Summary of testing.

Testing	Number of Specimens
Mass evaluation	32 (all specimens)
CT scanning	12 (one of each specimen type at each manufacturing process setting)
CT analysis	12
Structured light scanning	32
Surface roughness and cylindricity	4 (compression specimens only)
Mechanical testing	24 (mechanical specimens only)
SEM	12 (tensile fracture surfaces)

2. MASS EVALUATION

2.1 Method

Specimens were weighed using a Mittler analytical balance with a 261 g capacity and a resolution of 1×10^{-5} g. With proper calibration, this instrument is accurate to 0.1 mg. Each specimen was weighed five times, and the average value was reported.

2.2 Key Findings

No substantial mass differences were noted within each specimen set—tensile, compression, layer quality—considered in this study. Total mass of extrudate is not dependent on extruder stand-off distance for the specimens considered here. This is largely consistent with phase I findings.

2.3 Discussion

For this study, masses of specimens within a particular set (set denotes that specimens are of the same geometry and built at the same processing conditions) were remarkably consistent. Variability of specimens within a set is typically very small (standard deviations on the order of 10^{-2} g). Variation across manufacturing process conditions for a given specimen (example all tensile specimens in the tip to tray study) is also on the order of 10^{-2} g.

Figure 2 is a scatterplot comparing the mass of tensile specimens built at the four tip to tray distances considered in the study (optimal, 0.1 mm from optimal, 0.05 mm from optimal, –0.02 mm from optimal) with ground and flight tensile specimen masses. Similarly, figure 3 summarizes the compression specimen masses and figure 4 plots the layer quality specimens. A significant difference between the means of the specimen sets at the 95% confidence level for any group to group comparison was not detected. Specimens of the same geometry exhibit little variation in mass regardless of processing conditions. The complete list of specimen masses can be found in table 17 in the appendix.
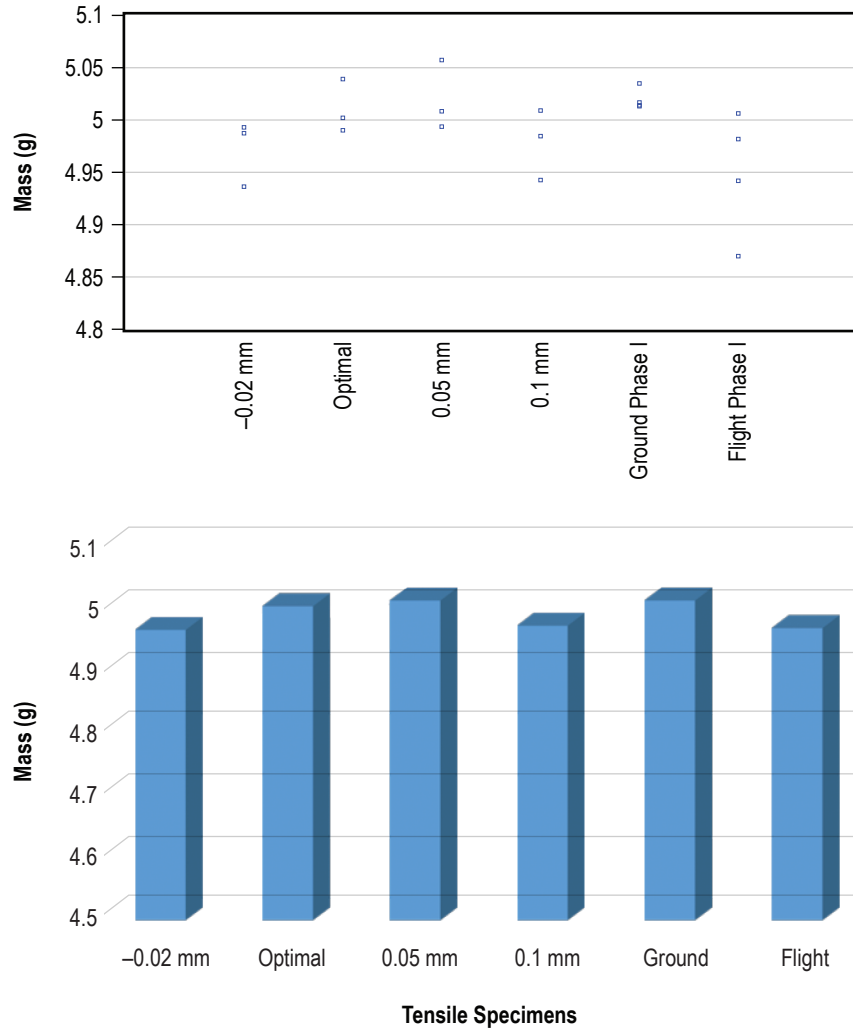
Figure 2. Scatterplot and bar graph comparing mass of tensile specimens for tip to tray study. Specimens from phase I ground and flight operations are plotted for context.
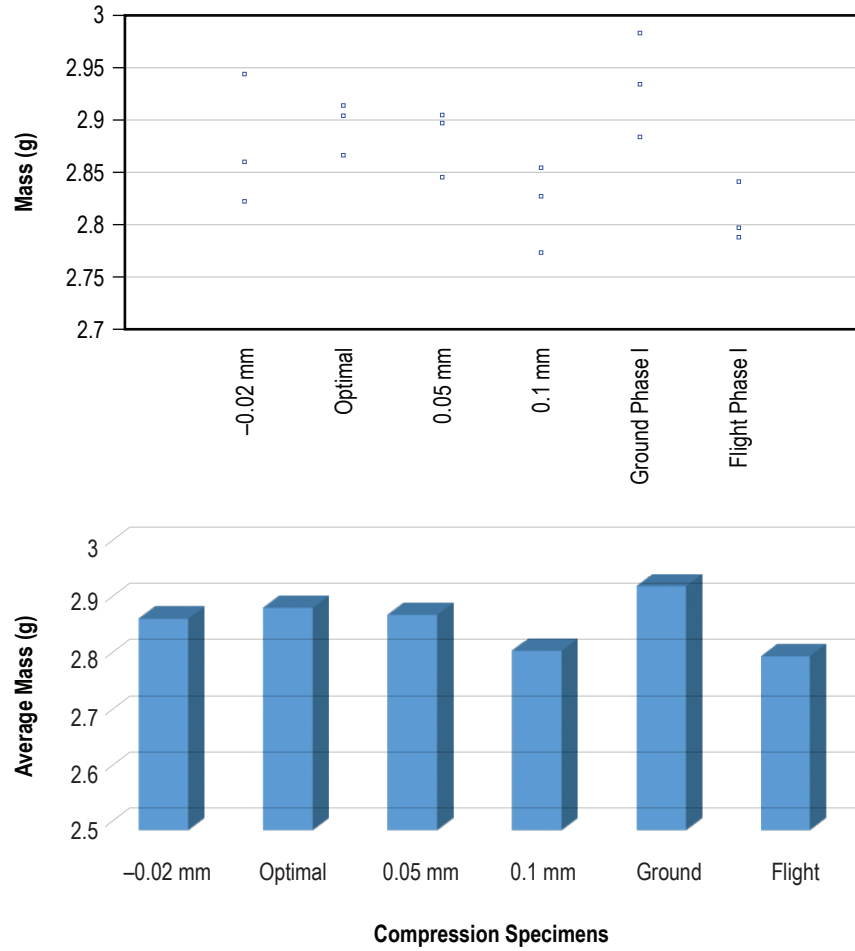
Figure 3. Scatterplot and bar graph comparing mass of compression specimens for tip to tray study. Specimens from phase I ground and flight operations are plotted for context.
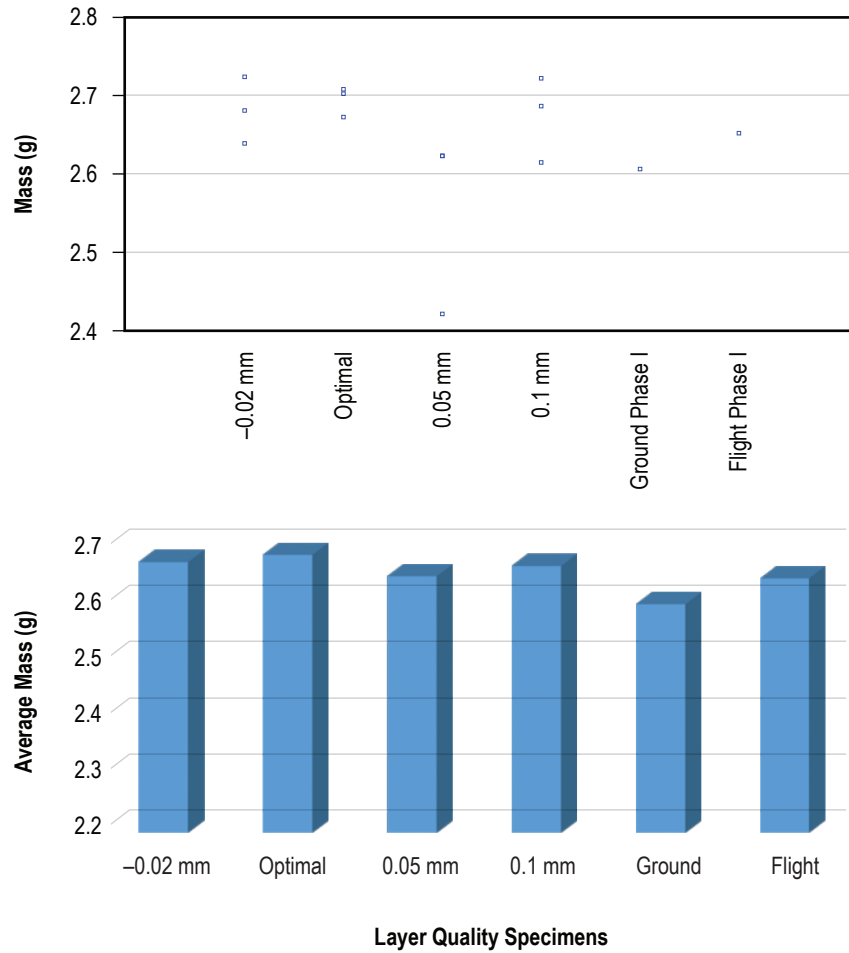
Figure 4. Comparison of mass of layer quality specimens for tip to tray study. Specimens from phase I ground and flight operations are plotted for context. Note that for ground and flight layer quality specimens, the average reported represents a single specimen (for all other classes $n = 3$).

3. DENSITY COMPARISON

3.1 Method

Volume of the closed part for each specimen was calculated from structured light scanning. The mass average value calculated from weighing of the specimens was divided by this volume to obtain the gravimetric density value.

3.2 Key Findings

A clear and consistent relationship between density and extruder standoff distance is not observed. For the compression specimens, the closest setting (0.1 mm) is in family with the lower density flight prints. Variability of specimens within a group (indicative of build to build variability for the 3DP hardware) may mask trends. Flight compression specimens from 3DP phase I are in family with specimens produced at the 0.1 mm setting, but they are also in family with other specimen sets in the extruder standoff distance study. Ground compression cylinders from 3DP phase I are distinct from all other specimen sets.

3.3 Discussion

Density was derived for each specimen from the mass measurement and the closed part volume calculated based on structured light scan data. Figure 5 compares the densities of the tensile specimens at various processing conditions in this study. Ground and flight phase I tensile specimens are plotted for comparison. Densities are highly variable for specimens within a given class, and there is no consistent relationship between density and the distance from the extruder at which the part is built. Ground phase I tensile specimens are distinct from all specimen sets and exhibit the lowest density.
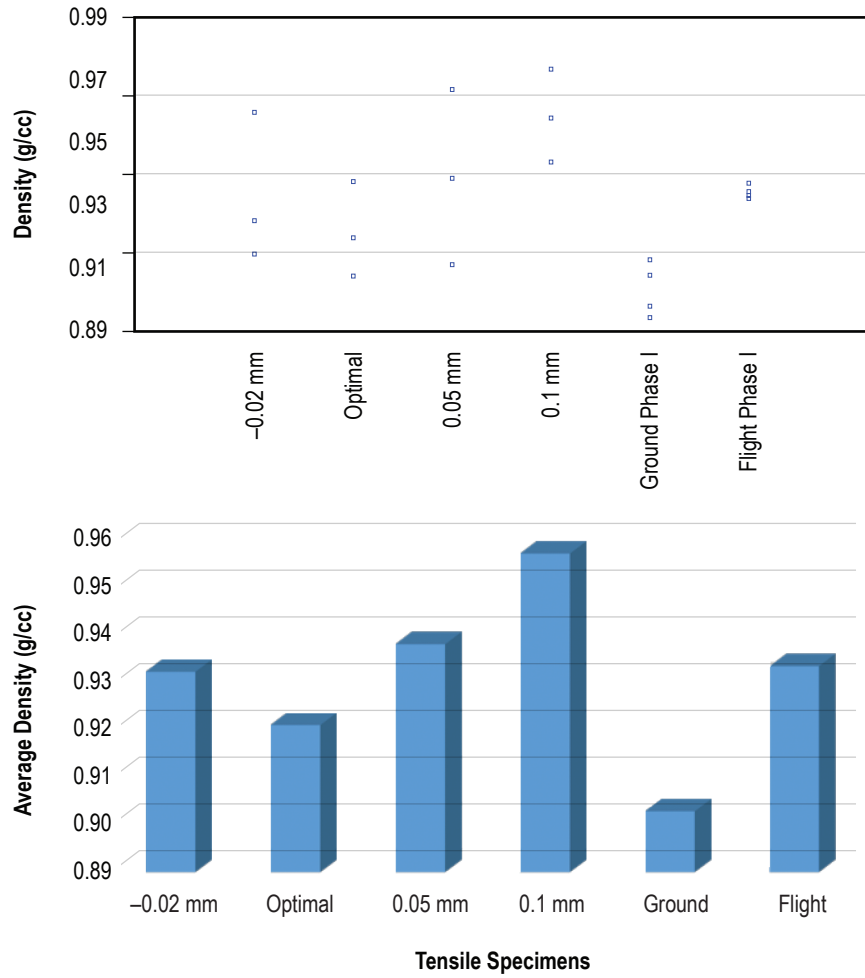
Figure 5. Density comparison of tensile specimens.

As seen in figure 6, compression specimens display a similar high degree of variability within specimen classes. Specimens built at the 0.1 mm processing condition are in family with the flight specimens. It is possible that building specimens at a setting that positions the build plate too close to the extruder can result in a slightly less dense compression cylinder.
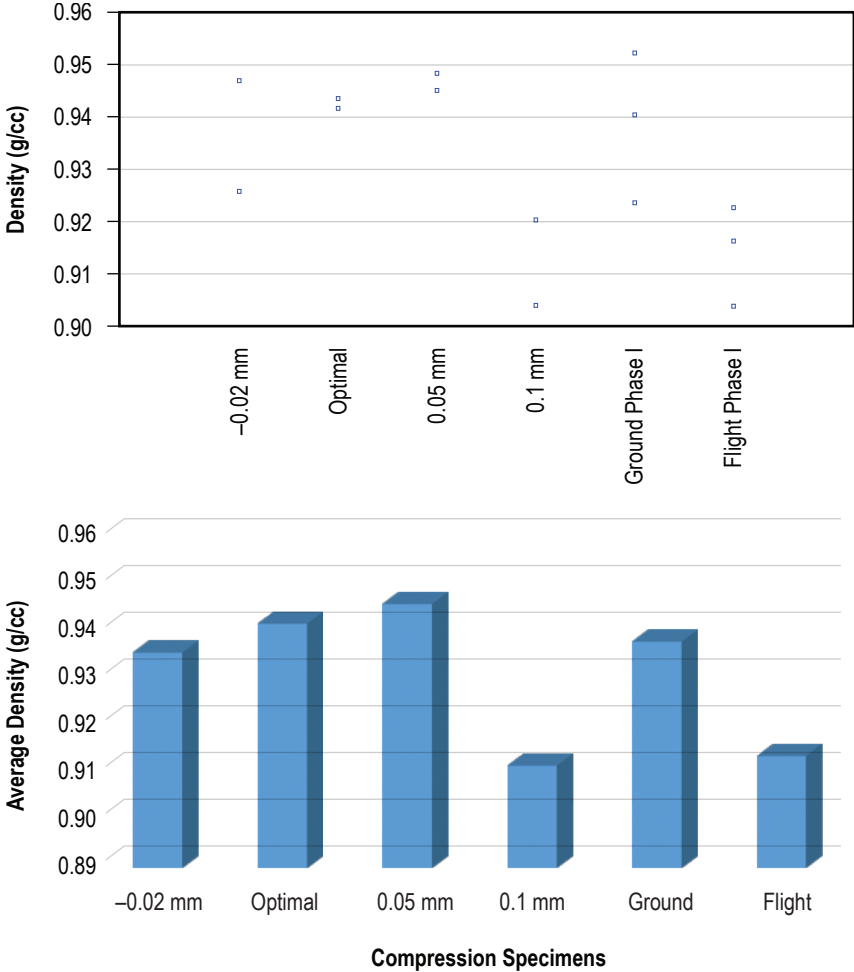
Figure 6. Density comparison of compression specimens.

For the layer quality specimens (fig. 7), the tip to tray distance seems to have no impact on densification. Additionally, it is difficult to situate the data within the context of the ground and flight phase I prints since there is only a single layer quality specimen for each round of ground and flight operations.
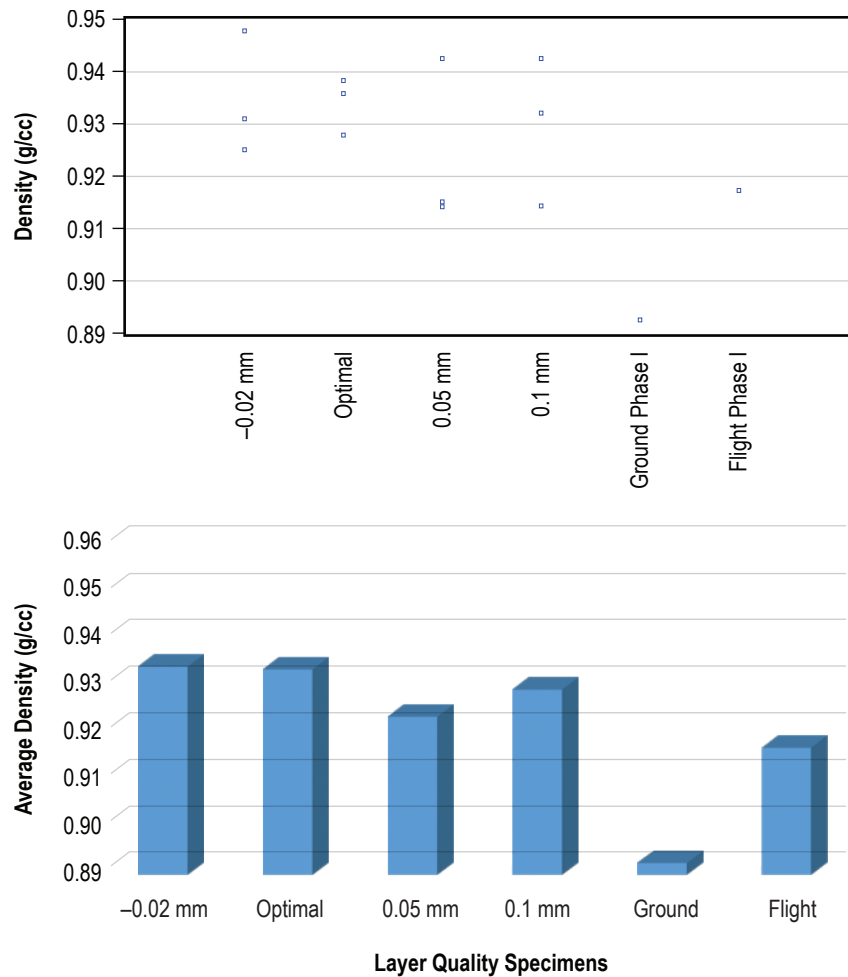
Figure 7. Density comparison of layer quality specimens. Note that for ground and flight layer quality specimens, the average reported represents a single specimen (for all other classes $n = 3$).

Figure 8 compares the density—irrespective of specimen type—across all manufacturing settings in the study. Each category on the *x*-axis includes all tensile, compression, and layer quality specimens produced at that condition. No groups in the tip to tray study are different at a statistically significant level in terms of density. Ground and flight specimens—each category includes tensile, compression, and layer quality—are plotted for comparison. Data are suggestive that build to build variability may overwhelm or obscure variability arising from differences in process settings or that densification is not dependent or extruder standoff distance over the range of values considered.

A tabular summary of density values is cataloged in table 18 in the appendix.
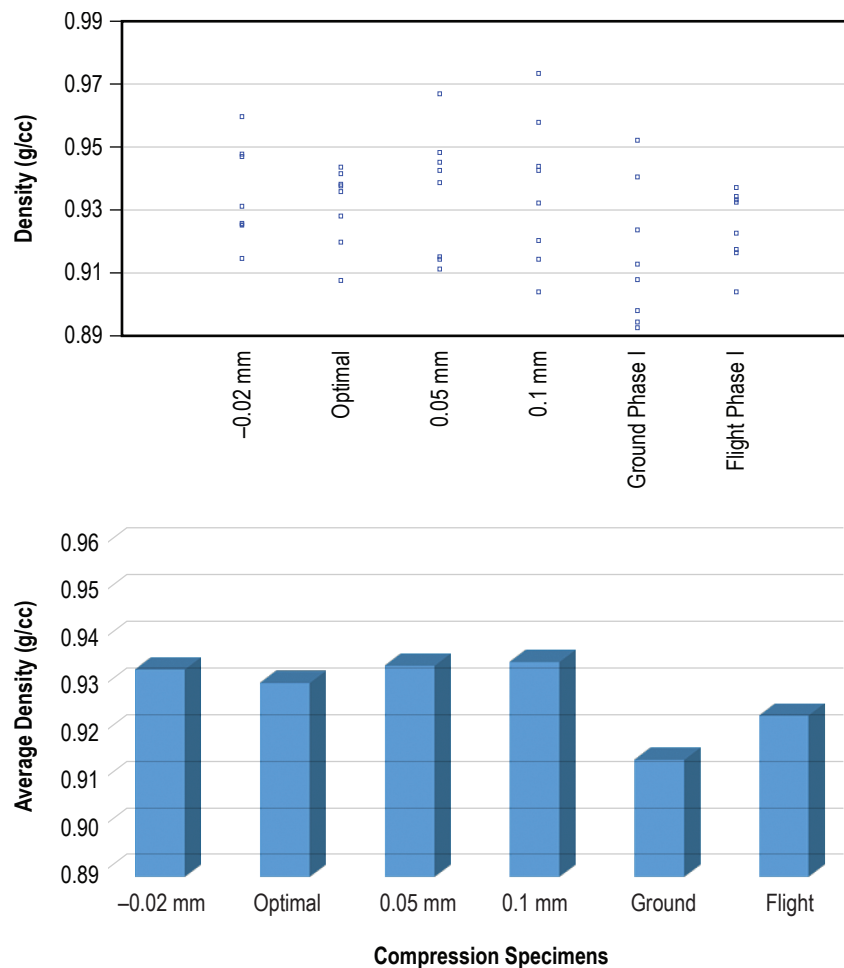
Figure 8. Comparison of density across tip to tray settings.

4. MECHANICAL PROPERTY COMPARISON

4.1 Method

Tensile specimens are type IV specimens from ASTM D638 and were tested per that standard.[5] Compression specimens were tested per ASTM D695 Standard Test Method for Compressive Properties of Rigid Plastics.[6]

4.2 Key Findings

Overall, ultimate tensile strength (UTS) and elastic modulus improve as the specimens are built closer to the extruder tip. This finding supports the hypothesis of the phase I results—that protrusions on the tensile specimens contribute to an artificial strengthening of the part which translates to enhanced mechanical performance relative to specimens built slightly farther away from the extruder tip that do not possess reinforcing structural features. These features align with the loading path during testing, contributing to increased mechanical performance.[3,7] The wide scatter of the fracture elongation data precludes a clear assessment of the relationship between extruder standoff distance and this metric.

A clear relationship between extruder standoff distance and material performance in compression was not detected by these experiments. The stronger mechanical behavior noted for the ground prints—built at a greater standoff distance—and comparatively weaker behavior of the flight prints—built at a smaller standoff distance—is not replicated in this data set.

4.3 Discussion

Tensile and compression coupons were mechanically tested in the Materials and Processes Laboratory at MSFC. Test procedures and test standards were identical to those used for the flight and ground specimens from the 3D printing in zero gravity (zero G) technology demonstration.

4.3.1 Tensile Test Results and Comparison

Tensile tests followed a standard method defined in ASTM D638[5] and measured the UTS, yield strength, elastic modulus, and fracture elongation of the printed material. Type IV specimens were selected to enable comparison with phase I ground and flight operations.

Tensile curves derived from specimens produced at each processing condition are plotted in figure 9. Individual plots for the three specimens at each condition can be found in figures 49–52 in the appendix. Tensile curves for ground and flight prints from 3DP phase I operations are plotted in figure 10 for comparison.
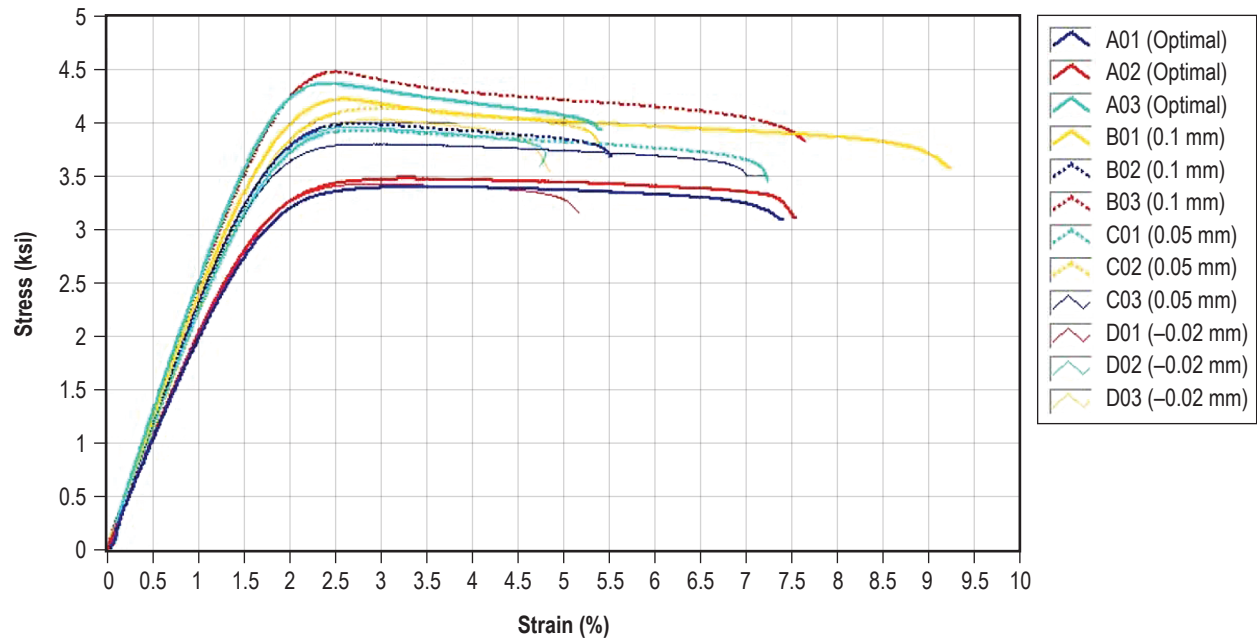
Figure 9. Tensile plot of all specimens in extruder standoff distance study.
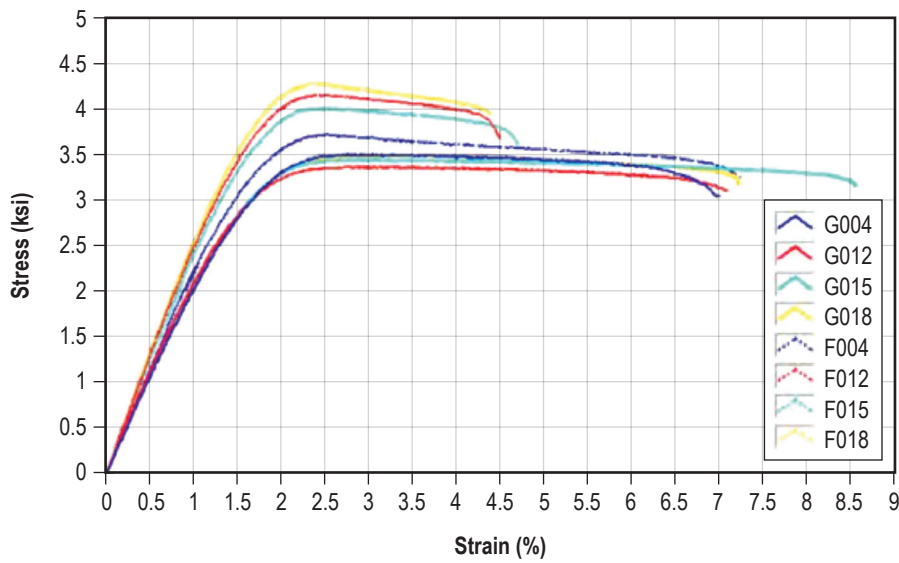
Figure 10. Plot of flight and ground tensile specimens from phase I. G designates ground specimen and F designates flight specimen.

Figures 11–13 compare the measured UTS, elastic modulus, and fracture elongation for materials made using the optimal 0.1 mm tip to tray offset (from the nominal value), 0.05 mm offset, and –0.02 mm offset. Data from phase I ground and flight specimens are plotted for comparison, although it is important to keep in mind that due to differences in the print trays, the processing conditions are approximate rather than identical. The 0.1 mm setting most closely approximates the flight prints and the –0.02 mm setting most closely approximates the condition for the phase I ground prints. A tabular summary of the data is provided in table 3. Accompanying bar charts in figures 11–13 serve as an additional visualization tool.
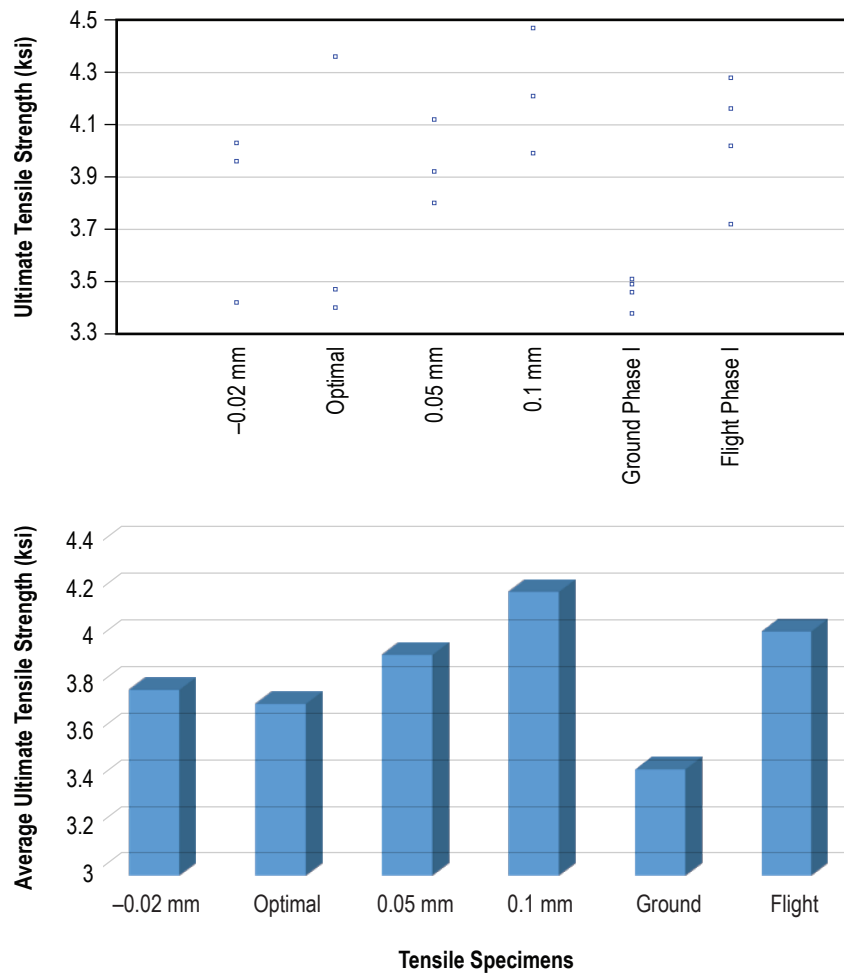
Figure 11. Scatterplot and bar chart comparing UTS for tensile specimens.
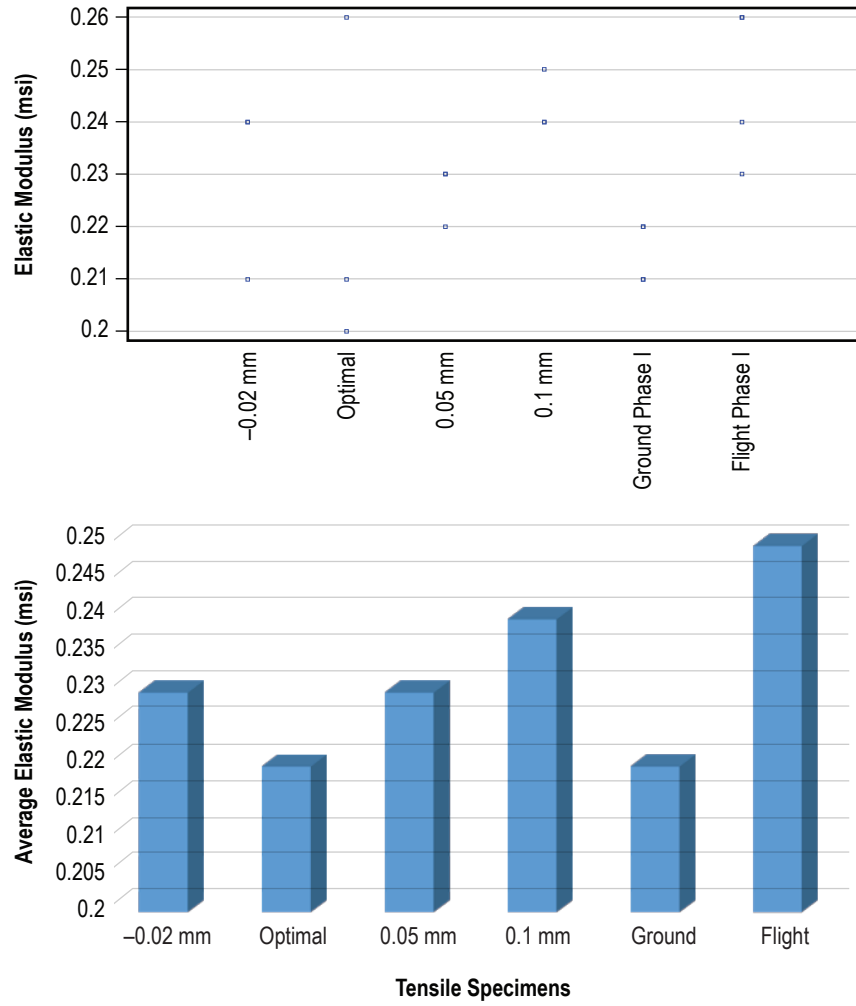
Figure 12. Scatterplot and bar chart comparing elastic modulus
   for tensile specimens.
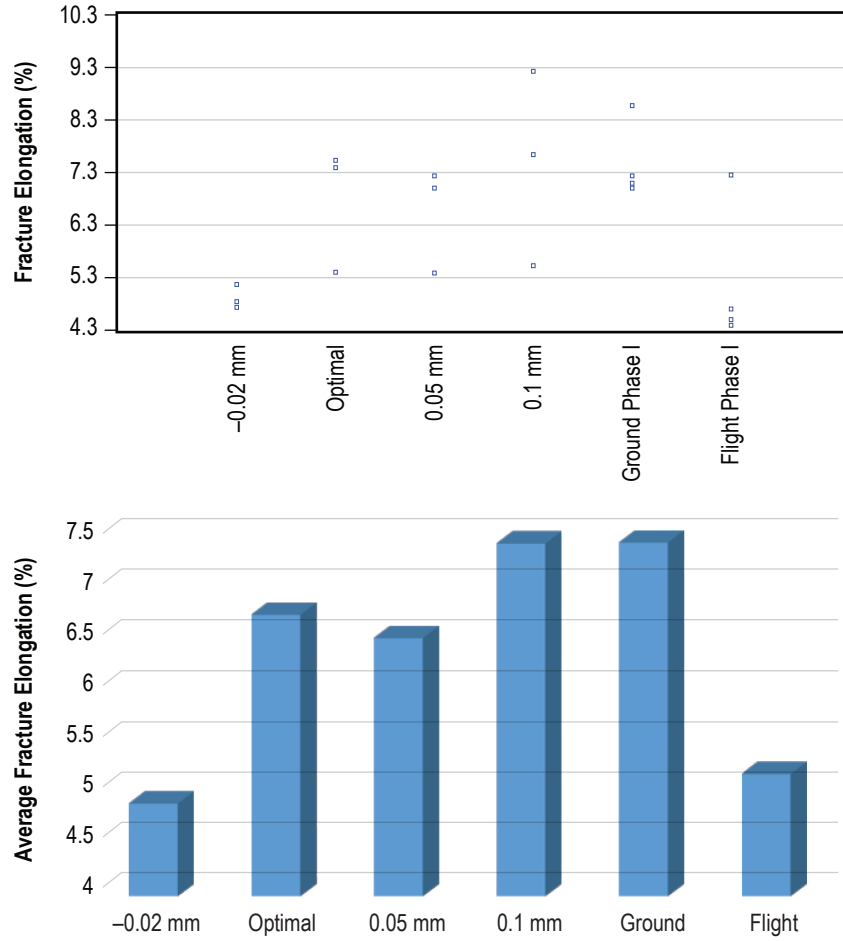
Figure 13. Scatterplot and bar chart comparing fracture elongation for tensile specimens.

Table 3. Summary of tensile test data.

Specimen Set	Mean UTS (ksi)	Coefficient of Variation (%)	Mean Elastic Modulus (msi)	Coefficient of Variation (%)	Mean Fracture Elongation (%)	Coefficient of Variation (%)
–0.02 mm	3.8	9	0.23	8	4.92	5
Optimal	3.74	14	0.22	13	6.77	18
0.05 mm	3.95	4	0.23	2	6.54	16
0.1 mm	4.22	6	0.24	3	7.47	25
Ground phase I	3.46	1.7	0.22	2.7	7.48	9.9
Flight phase I	4.05	6	0.25	6.1	5.21	26.3

Although it is difficult to see clear trending, due to the outlier in the optimal tensile specimen set, the mean of the UTS for the tip to tray specimens does increase as the extruder tip is moved closer to the build tray. The properties of the coupons within a specimen set are highly variable; as such, the classes do not exhibit a statistically detectable difference for the UTS metric. Specimens produced at the 0.05 mm and 0.1 mm processing conditions have a UTS that is most similar to values observed for the flight prints. (Both data sets are in family with the phase I flight specimens, although the sample sizes are small.) The –0.02 mm specimen set is in family with the ground prints from phase I. While a small number of specimens were considered, this trending could suggest that a too close print setting can strengthen the tensile specimen.

In general, modulus increases slightly with decreasing distance of the extruder tip from the build tray. As with UTS, the measured modulus for specimens at the 0.1 mm condition most closely resemble the flight specimens.

Fracture elongation data are highly variable for most data sets, and there is a large amount of overlap in the ranges of specimen classes. The –0.02 mm condition is not in family with the ground prints, and the 0.1 mm condition is not in family with the flight data. The wide scatter of the data precludes a clear assessment of the relationship between extruder standoff distance and fracture elongation for the 3DP hardware.

4.3.2 Compression Test Results and Comparison

Compression testing, per ASTM D695,[6] was used to determine the characteristic compressive stress and modulus of the specimens. Test procedures for this study deviated slightly from those used to evaluate the flight and ground specimens from the 3D printing in zero G technology demonstration in that the tests here were terminated when the compression specimens reached 20% strain. For the 3DP specimens, tests were run to 100% strain. This change in procedure was implemented to allow for better structural evaluation of the specimens and failure modes using SEM.

Compression plots for specimens at the –0.02 mm calibration condition, the optimal setting, 0.05 mm, and 0.1 mm appear in figure 14. Breakout plots of compression specimens at each processing condition appear in figures 53–56 in the appendix. Plots of compression specimen flight and ground prints are shown in figure 15, although it is important to keep in mind that the manufacturing settings for prints from the technology demonstration mission are not directly comparable with calibration settings considered in this study, due to the lack of closed-loop positional feedback information for the 3DP hardware and geometric differences in the build trays discussed in section 1. Ground prints broadly approximate the –0.02 mm condition and flight prints approximate the 0.1 mm setting.
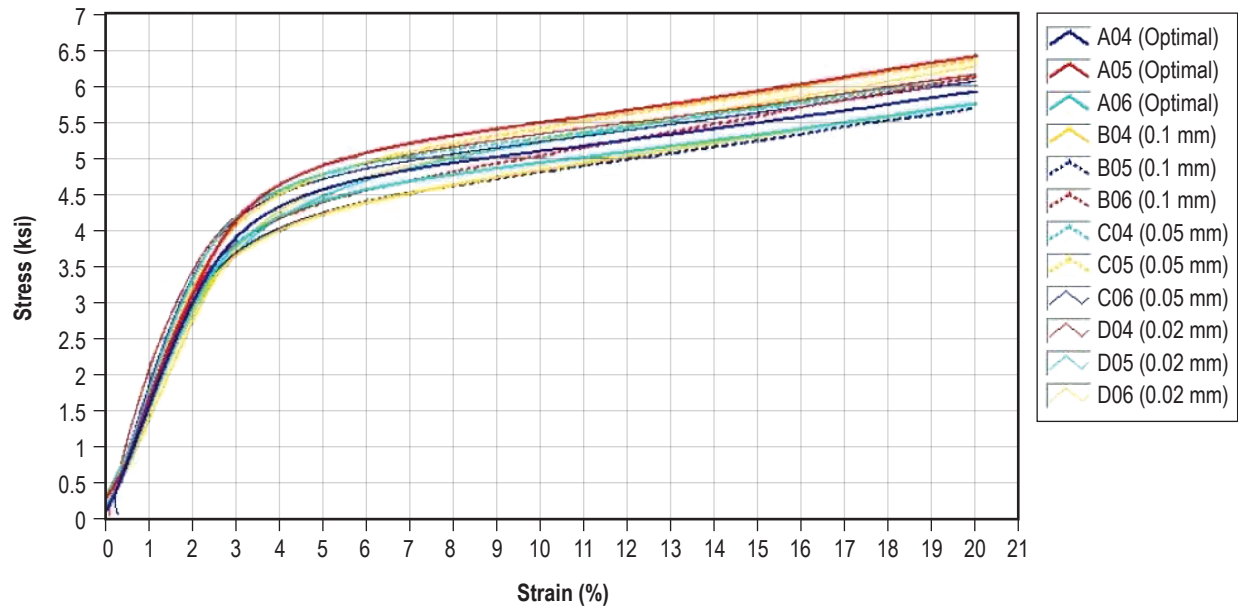
Figure 14. Consolidated plot of stress-strain curves for compression specimens across all manufacturing process settings.
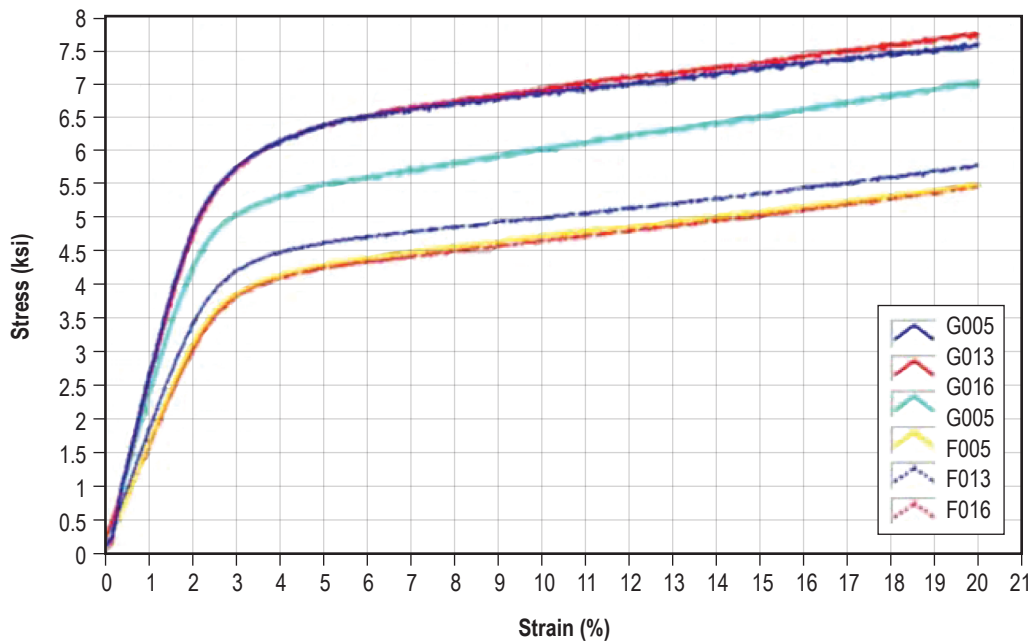
Figure 15. Stress-strain curves for compression specimens from 3DP phase I operations. G indicates ground specimen and F indicates flight specimen.

Figures 16 and 17 compare the measured compressive strength at 20% strain and compressive modulus, respectively, for materials made at the optimal, 0.1 mm tip to tray offset (from the nominal value), 0.05 mm offset, and –0.02 mm offset conditions. Data from phase I ground and flight specimens are plotted for comparison, although it is again important to keep in mind that, due to differences in the print trays, the processing conditions for ground and flight are only analogous—and not identical to—specimens at some of the conditions in the tip to tray study. The 0.1 mm setting most closely approximates the flight prints and the –0.02 mm setting most closely approximates the condition for the phase I ground prints. A tabular summary of the data is provided in table 4.
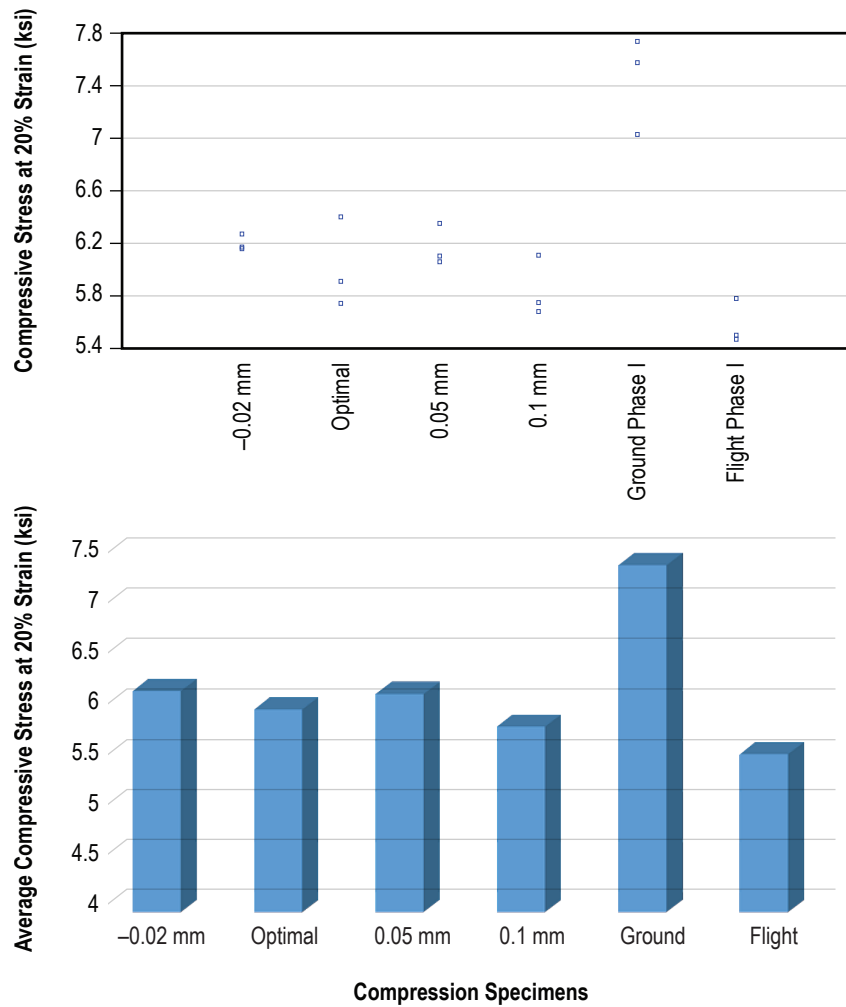
Figure 16. Scatterplot and accompanying bar chart comparing maximum compressive stress at 20% strain for specimen sets from tip to tray study and ground and flight prints from phase I operations of the technology demonstration mission.
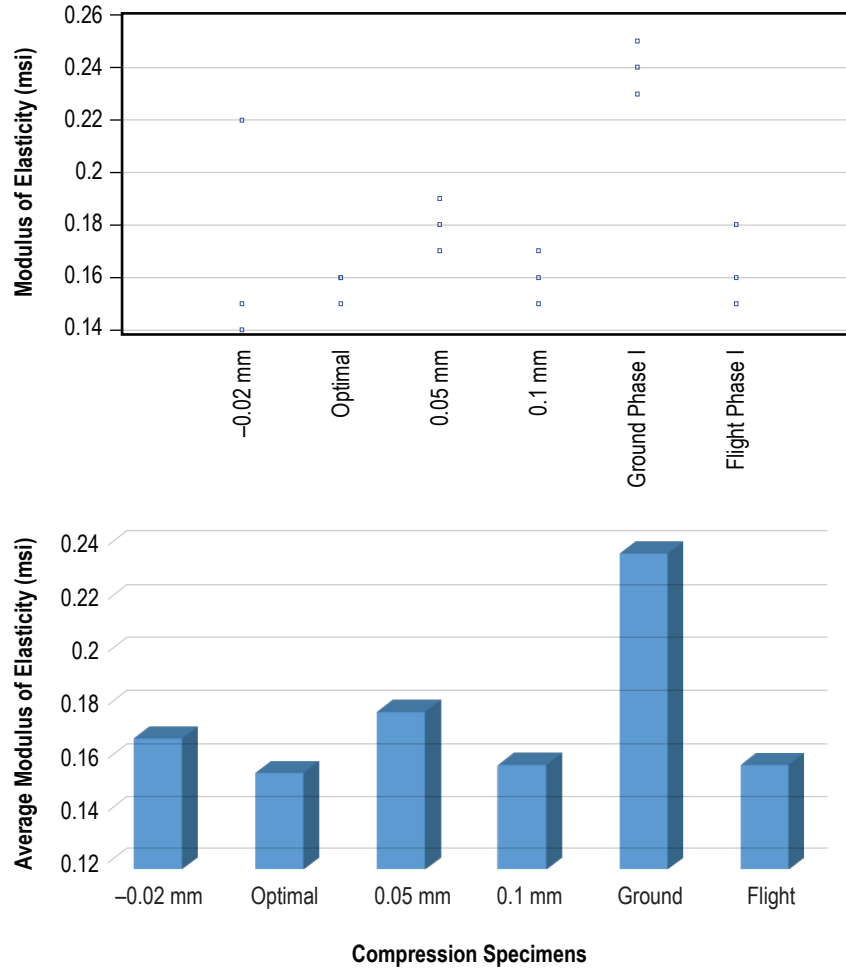
Figure 17. Scatterplot and accompanying bar chart comparing maximum compressive stress at 20% strain for specimen sets from tip to tray study and ground and flight prints from the technology demonstration mission.

Table 4. Summary of compression properties.

Specimen Set	Mean Compressive Strength (ksi)	CoV	Mean Compressive Modulus (msi)	CoV
–0.02 mm	6.2	1	0.17	25.6
Optimal	6.02	5.7	0.16	3.7
0.05 mm	6.17	2.6	0.18	5.6
0.1 mm	5.85	4	0.16	6.3
Ground phase I	7.45	5	0.24	3.1
Flight phase I	0.16	4.2	0.16	9.4

For compression specimens, clear trending in the variation of compressive properties and extruder standoff distance is not noted. The flight specimens, built with the extruder tip too close to the build platform, are the weakest in terms of compressive strength. The tip to tray specimen classes are in family with one another for compressive strength, regardless of processing conditions. All are distinct from the ground prints from 3DP phase I, with both the 0.1 mm and optimal processing conditions in family with the flight set.

Examining compressive modulus, all of the specimen sets from this study are also in family with one another, indicating that the variation in tip to tray distance over the range considered in this study ultimately has little impact on compressive properties. The –0.02 mm condition, which approximates the ground condition for 3DP phase I, is not in family with the ground specimens from 3DP, but is in family with the flight group.

Overall, a clear relationship between tip to tray distance and material performance in compression was not detected by these experiments. The stronger compressive properties noted for the ground prints and comparatively weaker behavior of the flight prints is not explained in terms of variation of the extruder distance (based on the manufacturing settings examined in this study).

5. STRUCTURED LIGHT SCANNING

5.1 Method

Structured light scanning creates a point cloud that can be used to characterize geometric variations in the surface of a part. Geometric data from a scan can be compared with the nominal computer-aided design (CAD) model or another part. Data from structured light scanning were also used to calculate the closed part volumes used in the calculations for gravimetric density reported in section 3.

MSFC performed structured light scans of all specimens in this study using the ATOS II, triple scan, blue light-emitting diode (LED) scanner. The scanner has an accuracy of ±12.7 µm at volumes on the scale of these parts. The scanner also captures stereoscopic images at a resolution of 5 million pixels per scan. The samples were coated in dry talcum powder, selected for its nonreactivity with the ABS plastic, to reduce the reflectivity of the sample surfaces and improve scan accuracy. The talcum powder grain size is approximately 10 µm in diameter, thus has little impact on scanner measurements.

The software package that accompanies the ATOS scanner uses the stereoscopic images to capture the fringe pattern sent out from the central LED projector. The software triangulates all of the surface data, using the grayscale pixels—black and white contrast from the fringe pattern—to determine the shape of the geometry. Through this process, the software generates a complete 3D model of the object being scanned. The software also provides real-time feedback to indicate missing surface data. Missing data are captured during subsequent scans.

The software package, Geomagic, compares virtual objects generated from the scans with the corresponding CAD model or another part model. Geomagic calculates dimensional variations from the 'reference' specimen. Geomagic also provides the volume of the printed parts from the scan data and makes geometric measurements of part features—length, height, diameter, etc.

5.2 Key Findings

As expected, the 'too close' calibration conditions of 0.1 mm and 0.05 mm exhibited greater protrusions than the nominal and 'too far' (–0.02 mm) settings. All samples exhibited slight warping. The batch of samples built in the too far condition showed extreme warping, with the most pronounced deformations in the tensile samples produced at this setting. The front paddle sections of the –0.02 mm batch of tensile samples lost contact with the build surface prematurely during printing, causing the upper layers to be compressed in the unadhered portions. These findings are remarkably consistent with observations from 3DP phase I specimens, indicating that slight variations in extruder standoff distance has a strong impact on form and geometry of the resultant specimen. Protrusions in the tensile specimens manufactured at the 0.05 mm and 0.1 mm condition could serve to strengthen the part by providing additional reinforcement material along the load path. Tensile specimens appear to be more susceptible to geometric variations resulting from differences in processing conditions. Specimen features and notable differences between specimen batches are given in section 5.3.

5.3 Discussion of Results

5.3.1 Protrusions

Comparison of the scan data shows a clear correlation between protrusions along the bottom edges of the samples and tip to tray distance. Several of the optimal calibration samples showed very slight protrusions, seen in the sample shown in figure 18. The too close conditions of 0.05 mm and 0.1 mm show progressively larger protrusions. The difference in protrusions among the batches of specimens is illustrated in figure 18. C01 and B01 (C specimens were printed at 0.05 mm condition and B specimens were printed at 0.1 mm) exhibit protrusions on the order of 0.01 inch and 0.02 inch, respectively. The too far condition (D01 in fig. 18) exhibited no protrusions along the bottom edge, but has some slight protrusions along the top edge. The upper layer protrusion is an artifact of the sample de-adhering from the build tray during the build process, resulting in compression of the upper layers.
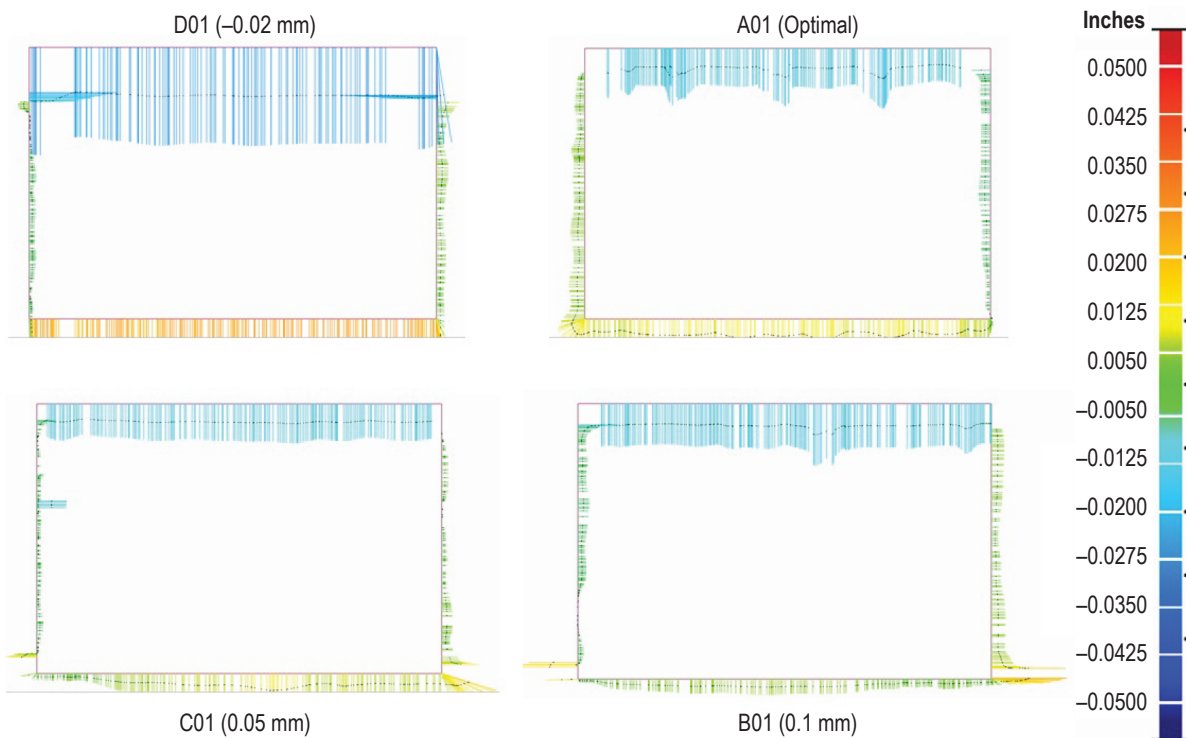
Figure 18. Two-dimensional cross sections of tensile test sections.

The increased incidence and magnitude of bottom edge protrusions as the extruder standoff distance decreases is not isolated to the tensile specimens. The compression and layer quality specimens both show the same trending. Figure 19 compares compression specimens built at the four processing conditions considered in the tip to tray study.
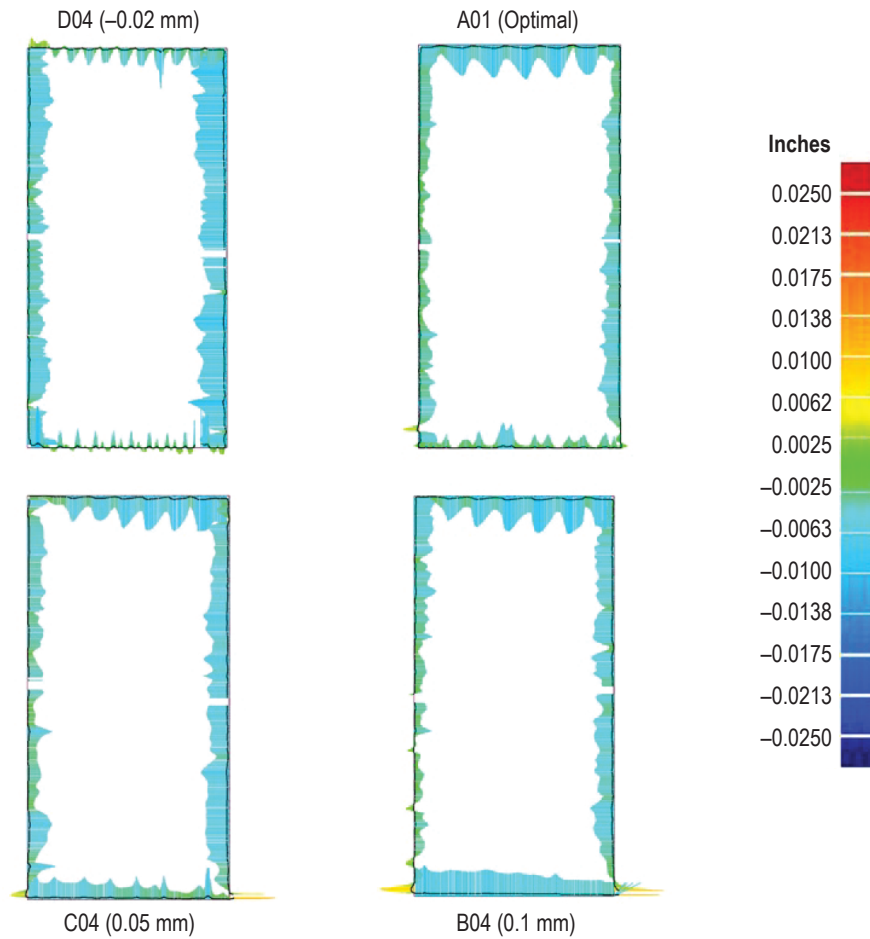
Figure 19. Two-dimensional cross sections of compression specimens.

5.3.2 Warping/Deformation

Analysis of the scan data indicate some degree of warpage or deformation in all of the specimens. This is likely a consequence of the uncontrolled thermal environment in the build chamber. The 3DP unit does not have a heated bed or heated volume, which is a feature of most commercial printers. Most notably, the majority of the sample surfaces are undersized. Part shrinkage is apparent in the compression specimens pictured in figure 19. Although still noticeable, warping of the specimens is extremely subtle in the compression and layer quality specimens relative to the tensile specimens, which have a much larger footprint in the x-y plane. A more detailed study of the bottom surfaces in figure 19 reveals progressively more erratic surface features as the extruder standoff distance increases. This appears to be a function of how well the extruded material adheres to the build surface.

Warping effects are more readily apparent in the tensile samples. The optimal and too close tensile samples (0.1 mm and 0.05 mm) showed slight warping. Warping is most likely induced by the prying force needed to remove the samples from the build surface and the internal stresses of

the samples as they are built in a nonheated build chamber/build surface. Figure 20 shows that the warping of the optimal, 0.05 mm, and 0.1 mm conditions are roughly the same, with about a 0.02-inch positive dimensional variation from the nominal CAD model between the ends of the paddle sections to the center of the test section.
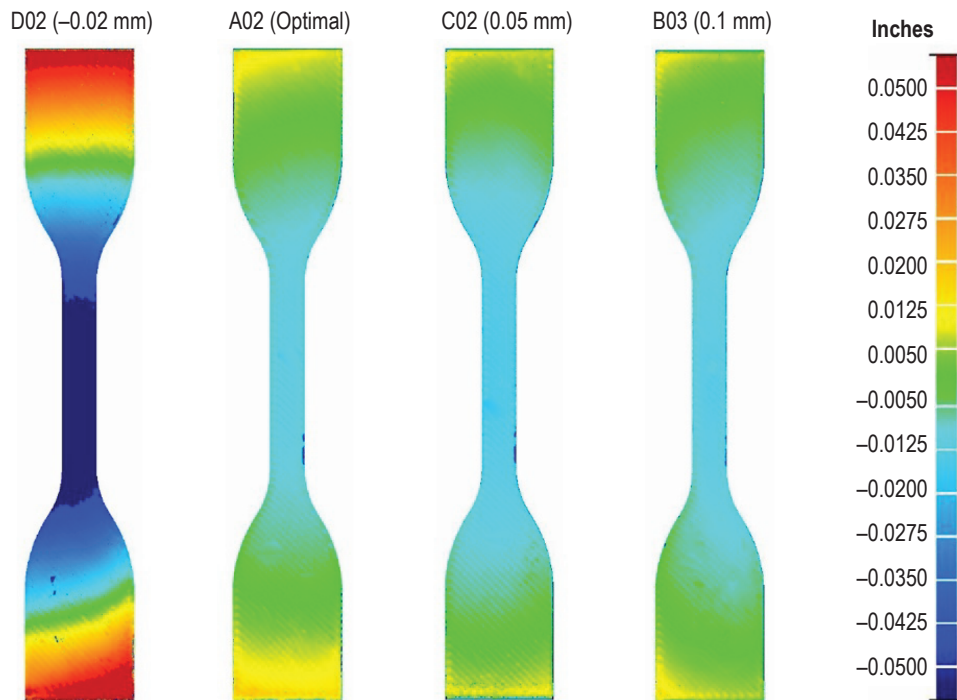
Figure 20. Top surfaces of tensile specimens.

The too far tensile samples exhibited the most exaggerated warping. Due to the poor adherence of the extrudate to the build surface, these samples tended to unadhere during the build in one of the two paddle sections. This, in turn, caused the upper layers to become compressed in the de-adhered portions. In figure 20, sample D02 shows a difference between the ends of the paddles to the center of the test section on the order of 0.1 inch, an order of magnitude larger than the degree of variation in the other specimens.

Basic geometric measurements were extracted from the scan data. The dimension of greatest interest for this study is the height of the specimen. Table 5 tabulates averages of the height measurements. The target height from the CAD model is tabulated for reference. These measurements indicate a correlation between height of the printed specimen and extruder standoff distance. For the tensile specimens, batches at 0.05 mm and 0.1 mm are progressively shorter than specimens produced at the optimal condition. The same relationship is apparent in the compression specimens but to a lesser extent. Layer quality specimens also become shorter with decreasing extruder standoff distance but, with the exception of specimens at the –0.02 mm condition, differences between specimen classes are on the order of tenths of thousandths of an inch. Based on these data, the variation

in specimen height from the nominal CAD model as a result of changes in extruder standoff distance become less pronounced as the height of the sample itself increases. This suggests that tensile specimens, which have a smaller height, are most susceptible to geometric variations resulting from processing conditions.

Table 5. Average height measurements of compression specimens from structured light scanning.

Average Height Measurements (inches)			
Batch	Tensile	Compression	Layer Quality Specimen
CAD height	0.1575	1	1.1811
−0.02 mm	0.1545	0.9979	1.1822
Optimal	0.1547	0.993	1.1807
0.05 mm	0.15	0.9918	1.18
0.1 mm	0.1452	0.9909	1.1802

6. X-RAY/COMPUTED TOMOGRAPHY

6.1 Method

Computed tomography imaging was performed with a microfocus x-ray tube and digital detector panel. The output consists of CT slices and a reconstructed data volume representing the radiographic density and geometric configuration of each sample. Solid acrylonitrile butadiene styrene (ABS) disks of known density were scanned alongside the sample to provide a reference value for the CT density number. The CT number is a unitless measurement that represents the combined influence of physical density and x-ray absorption in the cross section of the sample material. The CT number is expressed as a proportion of known physical density of the solid ABS. Analysis of the data for each scanned specimen was performed using Volume Graphics VGStudio software.

The analyzed samples fell into three categories:

(1) Cylindrical compression test specimens (specimen numbers A4, B4, C4, and D4).
(2) Rectangular tensile test specimens (specimen numbers A01, B01, C01, and D01).
(3) Layer quality (columnar) specimens (specimen numbers A7, B7, C7, and D7).

As in the other testing phases, A class specimens correspond to the optimal calibration value, B is the 0.1 mm condition, C is the 0.05 mm calibration setting, and D is the –0.02 mm standoff distance.

Computed tomography numbers calculated for each specimen were compared against those collected from a solid, conventionally manufactured (via injection molding) disk of ABS that was scanned in the same CT inspection for the compression and layer quality specimens. The ratio of CT numbers for the printed material to those for the solid material should correlate linearly to the difference in bulk physical densities between the two materials. An estimate of the bulk physical densities of the printed part can be obtained by multiplying the calculated ratio of CT densities by a known density of the solid ABS obtained by other means, or by using a textbook value.

No ABS disk was included in the scans of the tensile specimens (category 2), which were scanned at a lower x-ray energy (100 keV) than those used for categories 1 and 3. For reference purposes only, the tensile specimen CT numbers (inspected at 100 keV) were compared to the mean CT numbers for solid ABS obtained from category 1 (compression specimen) scans performed at 120 keV x-ray energy. The CT numbers for solid ABS scanned at 100 keV should not be significantly different from those that would be obtained from scanning the same material at 120 keV. It is expected that the actual 120 keV scan CT numbers for ABS would be slightly lower than CT numbers that would have resulted from scanning the solid ABS at 100 keV. Therefore, estimated densities for the printed tensile specimens with respect to solid ABS may be slightly lower than their actual physical densities. Any estimated bulk physical densities of the tensile specimens that are used or published should include a caveat to this effect.

Review of the individual CT slices revealed a large number of features that may not be detrimental to performance or integrity of the printed hardware. These features have not been characterized as defects. Rather, they are evident irregularities or anomalies that are visible in CT and fall into one of four categories:

(1) Voids: Rounded gaps in printed layers that may persist vertically in the z-direction (usually the symmetry axis of the printed part).

(2) Missing material: Evident interruptions of otherwise nominal material deposit along a print line that are not rounded.

(3) Misruns: Print lines that cross over adjacent lines.

(4) Foreign object debris, inclusions, or high density inclusions (HDIs):

(a) Particles of higher or lower density that are either attached to the outside surface (categorized as foreign object debris (FOD)).

(b) Inclusions, nearly all higher than the baseline ABS density, that were categorized as either inclusions or HDIs. (These terms were used interchangeably through the analysis of various specimens.)

It must be emphasized that none of these features are known to be a defect that could impact material performance. They were instead identified for their apparent deviation from observed baseline material uniformity and/or geometry. They have been documented in this TP for the purpose of assisting either the diagnosis of performance variations in mechanical testing or characterizing the performance of the varying printing parameters used to produce the specimens.

6.2 Key Findings

No consistent relationship in bulk density and extruder standoff distance for compression and layer quality specimens was detected based on quantitative CT data. Clear trending is apparent in the tensile specimens, as mean CT (and the bulk density calculated based on this value) of the tensile coupon increases as the extruder tip moves closer to the build tray. This is likely due to the formation of protrusions (excess material at the base of the part). These protrusions function as material reinforcements in the direction of loading that could contribute to slightly enhanced mechanical performance.

Qualitative comparison of representative images from the CT volumetric scans across manufacturing processing conditions serve to substantiate the hypothesis that a reduced extruder standoff distance improves tensile performance in the manner observed for the 3DP phase I flight prints. Examination of compression specimens and layer quality specimens does not show a strong relationship between the internal material structure and the z-calibration setting, although the larger 'gaps' between layers of material noted for the 0.1 mm compression specimens are a structural feature that could contribute to premature failure relative to other specimens with less spacing. This statement

is speculative, and controlled studies on void distribution would be needed to better understand whether such a relationship exists. Several misruns—print lines that cross over adjacent lines—were noted for the compression specimens and suggest that contours in specimen geometry may pose a challenge for this particular printer.

6.3 Comparison of Mean Computed Tomography Numbers and Densities

6.3.1 Compression Specimens

Table 6 summarizes the mean CT numbers for the four compression specimens—one at each manufacturing process setting—that underwent CT. A more detailed procedure for analysis of a specimen and calculation of relative density compared to solid ABS can be found in the appendix. Sides 1 and 2 correspond to different regions of the specimen, roughly dividing the specimen in half for each calculation. Differences between these regions are small for the optimal processing condition and for the 0.05 mm offset distance, but are larger for the distances at the extremes of the processing envelope—the closest distance of 0.1 mm and the farthest distance of –0.02 mm. Computed tomography bulk densities are generally about 10% greater than the density values derived from structured light scanning and mass measurement data. There is reasonable agreement between bulk density derived from CT and gravimetric density based on structured light scan data and specimen mass measurements. Gravimetric density is consistently slightly less than density calculated from CT.

Table 6. Mean CT numbers for compression specimens.

	Process Setting	Bulk Sample	Bulk ABS	Ratio to ABS	Bulk Density (g/cc)*	Gravimetric Density (g/cc)**
A4 side 1	Optimal	0.0216	0.023	0.939	0.986	0.9416
A4 side 2	Optimal	0.0216	0.023	0.938	0.985	0.9416
B4 side 1	0.1 mm	0.0219	0.0227	0.963	1.011	0.9203
B4 side 2	0.1 mm	0.0205	0.0227	0.904	0.949	0.9203
C4 side 1	0.05 mm	0.0219	0.0231	0.95	0.997	0.9451
C4 side 2	0.05 mm	0.0217	0.0227	0.957	1.004	0.9451
D4 side 1	–0.02 mm	0.0225	0.0228	0.986	1.035	0.947
D4 side 2	–0.02 mm	0.0217	0.0231	0.939	0.986	0.947

*Bulk density calculated based on textbook density value for injection molded ABS of 1.05 g/cc.
**Gravimetric density calculated based on closed part volume from structured light scanning and mass measurement.

The bar chart in figure 21 compares the bulk density of the specimens derived from CT across the manufacturing processing conditions considered in the study. The reported value is the average of side 1 and side 2 for each specimen. There is very little difference in bulk density across the stand-off distances. There is also not a consistent trend or discernable relationship between density and standoff distance for the compression specimens. This finding corroborates the comparison of the gravimetric densities across manufacturing process settings. One additional limitation is that only one specimen of each class (tensile, compression, layer quality) was scanned at each level (optimal,

0.1 mm, 0.05 mm, and –0.02 mm). If more specimens were scanned at each manufacturing setting, then trends in the data could emerge that are not apparent with a single specimen. However, the gravimetric density comparison discussed previously, which included a density value for every specimen, is not suggestive of a clear and consistent relationship, even with additional data points.

Figure 21. Bulk density calculated based on CT and manufacturing process setting for the analyzed compression coupons.

6.3.2 Tensile Specimens

Table 7 summarizes the mean CT data for the tensile specimens. Because the tensile specimens exceed the dimensions of the scan window for the CT tube, half of each specimen—identified as side A or side B—was scanned separately. There are no substantive differences in the mean CT values for the sides of a given specimen. The bar chart in figure 22 shows the average bulk density for a tensile specimen at a particular manufacturing setting. Bulk ABS data, in this instance, is derived from the injection molded specimen that was scanned alongside the compression specimens. Bulk density is calculated from CT data by multiplying the ratio or the specimen mean CT to the mean CT of ABS by the density of injection molded ABS.

Table 7. Mean CT numbers for tensile specimens.

	Process Setting	Bulk Sample	Avgerage Bulk ABS	Ratio to ABS	Bulk Density (g/cc)*	Gravimetric Density (g/cc)**
A01 side 1	Optimal	0.0203	0.0229	0.888	0.932	0.9197
A01 side 2	Optimal	0.0201	0.0229	0.88	0.924	0.9197
B01 side 1	0.1 mm	0.0211	0.0229	0.922	0.968	0.944
B01 side 2	0.1 mm	0.021	0.0229	0.917	0.963	0.944
C01 side 1	0.05 mm	0.0201	0.0229	0.879	0.923	0.9111
C01 side 2	0.05 mm	0.0205	0.0229	0.897	0.942	0.9111
D01 side 1	−0.02 mm	0.02	0.0229	0.873	0.916	0.9145
D01 side 2	−0.02 mm	0.02	0.0229	0.873	0.916	0.9145

*Bulk density calculated based on 1.05 g/cc density value for injection molded ABS.
**Gravimetric density calculated based on closed part volume from structured light scanning and mass measurement.

Figure 22. Bulk density calculated based on CT and manufacturing process setting for the analyzed tensile coupons.

Although the CT data set is limited, there is a clear trend in the tensile data in relation to bulk density—specimens become denser as the standoff distance between the extruder and the build plate decreases. This is also reflected in the gravimetric density values, but to a lesser extent. There is good agreement between bulk density derived from CT and gravimetric density based on structured light scan data and specimen mass measurements.

6.3.3 Layer Quality

Computed tomography data for layer quality specimens is summarized in table 8. Mean CT data for two regions of each specimen are provided. Variations in within-specimen densities are not substantial with the exception of the 0.1 mm condition, where side one is approximately 8% greater than side two. Bulk density of a layer quality specimen at each manufacturing process condition is plotted in figure 23. As with the gravimetric density comparison (which included more data points), there is no clear trend in variation of bulk density with extruder standoff distance from the build tray.

Table 8. Computed tomography data for layer quality specimens.

	Process Setting	Bulk Sample	Bulk ABS	Ratio to ABS	Bulk Density (g/cc)*	Gravimetric Density (g/cc)**
A7 side 1	Optimal	0.02090373	0.02217912	0.942495915	0.98962071	0.9383
A7 side 2	Optimal	0.02094738	0.02198125	0.952965823	1.00061411	0.9383
B7 side 1	0.1 mm	0.0198878	0.02249811	0.883976476	0.9281753	0.9322
B7 side 2	0.1 mm	0.02141197	0.02270929	0.942872719	0.99001635	0.9322
C7 side 1	0.05 mm	0.02001202	0.022818	0.877027785	0.92087917	0.9143
C7 side 2	0.05 mm	0.02037426	0.02291526	0.889113194	0.93356885	0.9143
D7 side 1	–0.02 mm	0.02065608	0.02288341	0.902666167	0.94779948	0.9311
D7 side 2	–0.02 mm	0.02035078	0.02295119	0.88669825	0.93103316	0.9311

*Bulk density calculated based on 1.05 g/cc density value for injection molded ABS.
**Gravimetric density calculated based on closed part volume from structured light scanning and mass measurement.
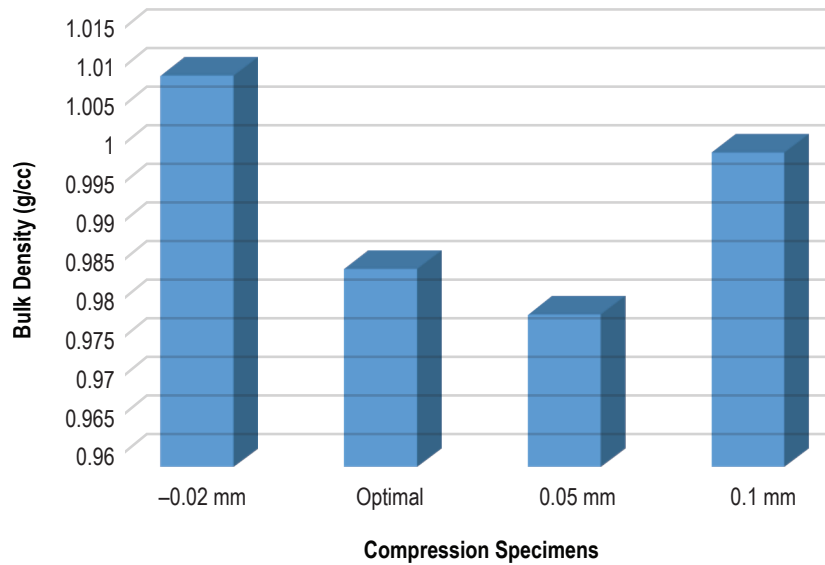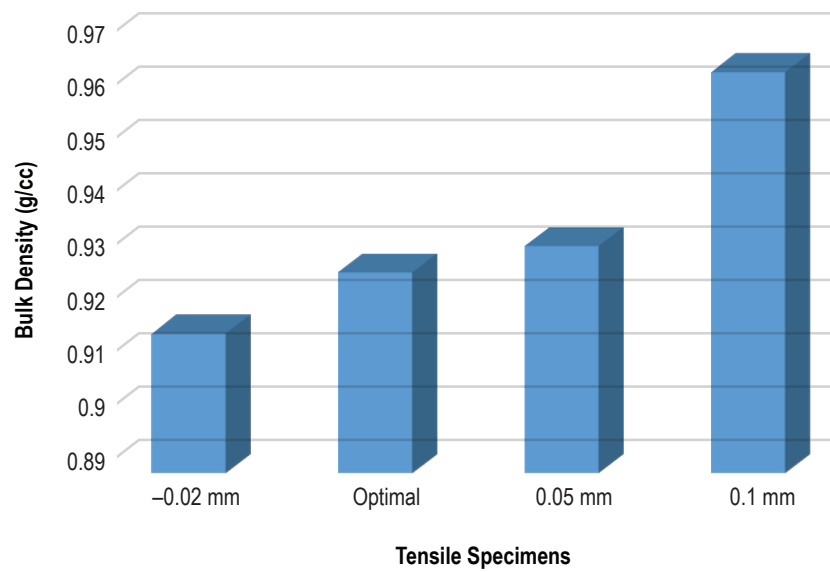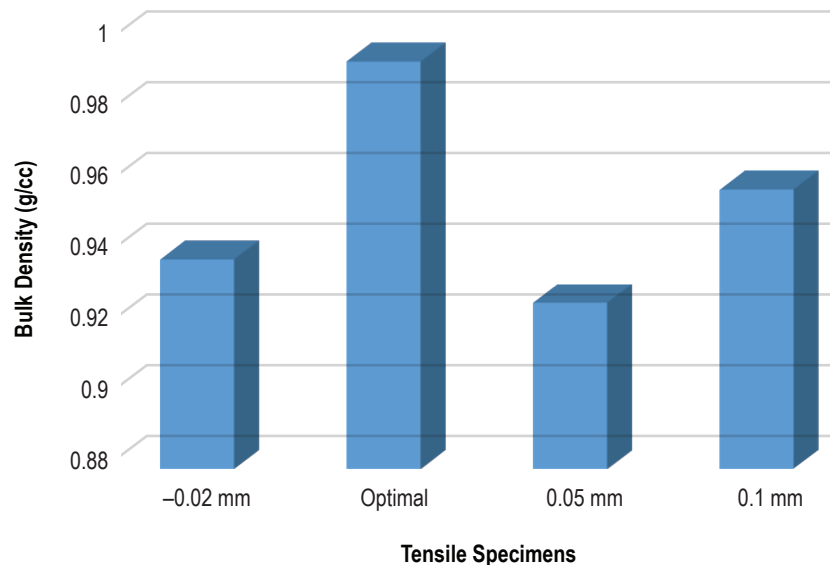

Figure 23. Bulk density calculated based on CT and manufacturing process setting for the analyzed tensile coupons.

6.4 Key Features of Specimens

6.4.1 Tensile Specimens

Slice images of tensile specimens reveal FOD on the edges of the part. Internal FOD is observed in specimen D01, voids on the edges of the specimens and in the interior, and several instances of low density indications (LDIs). These features are not classified as defects, since it is not clear that they impact mechanical performance.

Voids are inherent to the FDM process. However, there is a notable difference in size and frequency of voids for the tensile specimens based on the standoff distance for the part during the manufacturing process. For example, specimen D (manufactured at the –0.02 mm process setting, which is the farthest the extruder tip is from the build tray for specimens in this study) has voids uniformly distributed throughout and an 'open' material structure consistent with its lower mechanical performance (fig. 24) In contrast, specimen B's (0.1 mm) setting produces a denser structure relative to the –0.02 mm setting, but also has some low density indications in the upper half of the specimen (fig. 25). The protrusions at the base of the specimen, characteristic of a closer standoff distance, are also clearly visible in the slice image in figure 25.
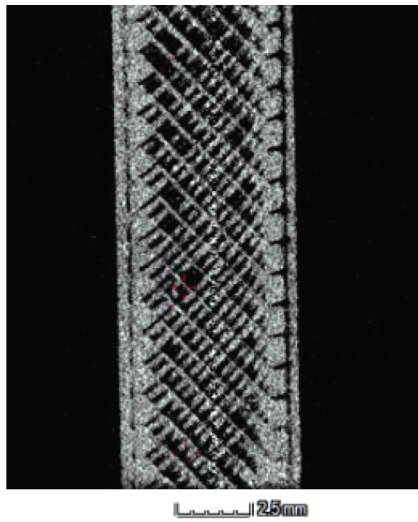
Figure 24. Tensile specimen at –0.02 mm manufacturing process setting. Image in *x-y* plane
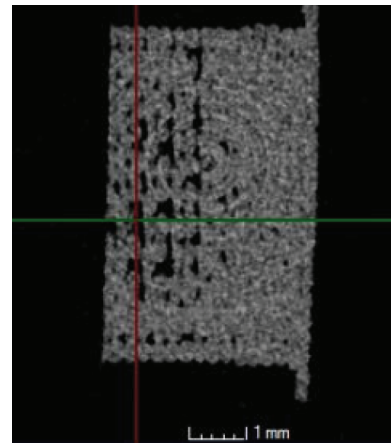
Figure 25. Slice image of *y-z* plane for tensile specimen at 0.1 mm manufacturing process setting.

The evolution of the material density with decreasing standoff distance can be seen in figure 26. Images progress from the open specimen in image (a) (–0.02 mm) to the densest specimen in (d) (0.1 mm). These results parallel the changes in material structure observed in the tensile specimens for phase I, where ground specimens—built with the extruder tip too far away—had an open structure with distributed void space and flight specimens (generally built with the extruder tip too close) were comparatively denser with reinforcing agglomerations and protrusions near the base of the specimen.
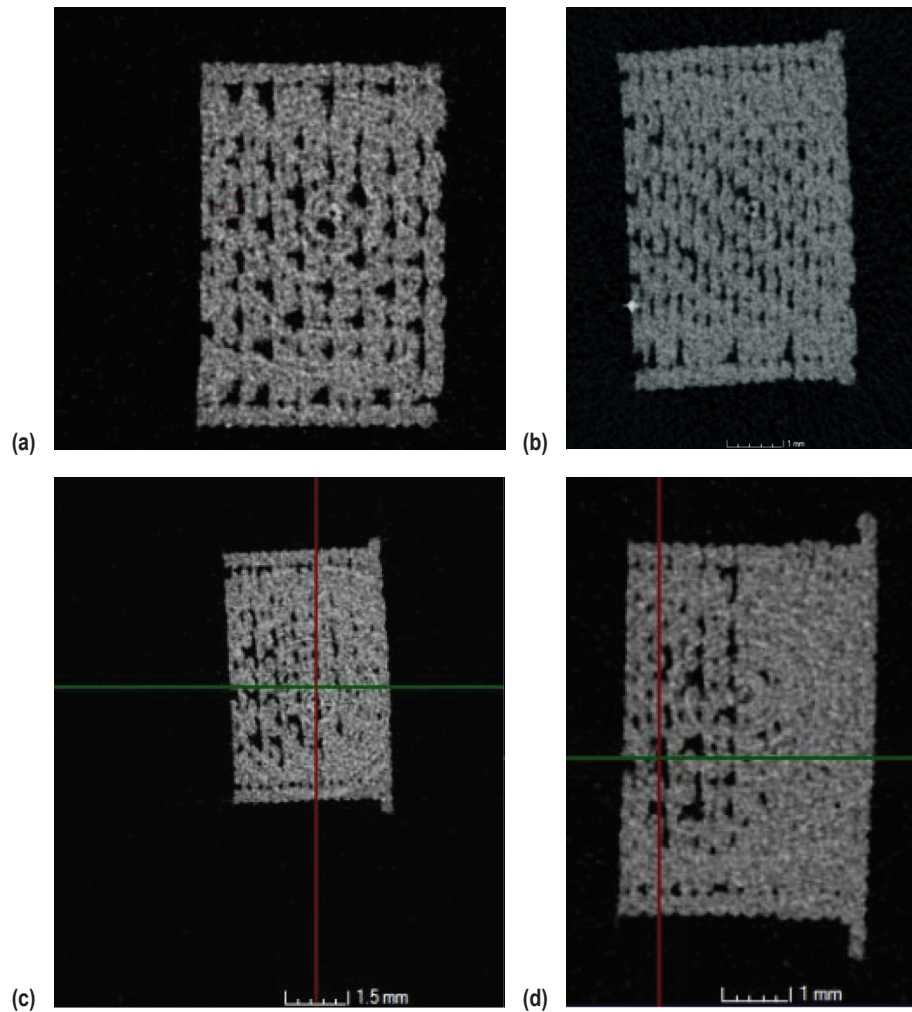
Figure 26. Computed tomography images showing evolution of material structure of tensile specimens with differences in manufacturing standoff distance: (a) –0.02 mm offset, (b) optimal condition, (c) 0.05 mm offset, and (d) 0.1 mm offset.

On some specimens, FOD was detected on the outside of the specimens. There was one instance of embedded FOD (specimen D01). FOD is likely an artifact of specimen preparation for structured light scanning, where specimens are sprayed with a talcum powder and targets with adhesive are applied to the specimen. The targets are removed and specimens are blown with air to remove powder, but the porous nature of the parts can result in powder entrapment.

6.4.2 Compression Specimens

Previously, no clear and consistent trends in variation of density or mechanical performance with extruder standoff distance for the compression specimens were noted. Visually, the CT images of compression specimens at all manufacturing process settings resemble one another. In illustration of this point, figure 27 compares CT slices at the –0.02 mm offset, optimal condition, 0.05 mm offset, and 0.1 mm condition. Compression specimens have the greatest bulk density of the specimen classes. No stepwise change in density occurring at approximately the midpoint of the specimen in the z-direction was noted. (This abrupt density change, visually apparent on CT of the ground and flight specimens from phase I operations of the 3DP in zero G technology demonstration mission, was ultimately determined not to be statistically significant based on comparison of mean CT numbers.) For the compression specimens in this study, size and frequency of voids is broadly consistent across extruder standoff distances. The specimen built at the 0.1 mm condition is structurally distinct from the other specimens in that there are a number of 'air gaps'—a series of consecutive void spaces—which run along the z-axis of the specimen in the direction of the build. These can be seen, to some extent, in the other specimens, but the patterns of voids are more visually dramatic and have a longer length in the 0.1 mm class specimen. The specimen at this condition, however, has a greater bulk density than specimens at the 0.05 mm and optimal settings. (Specimens (b) and (d) appear to have a more closely packed material structure.) It cannot be determined from this data set whether extruder standoff distance explains the differences in mechanical performance between the flight and ground compression specimens from 3DP phase I.
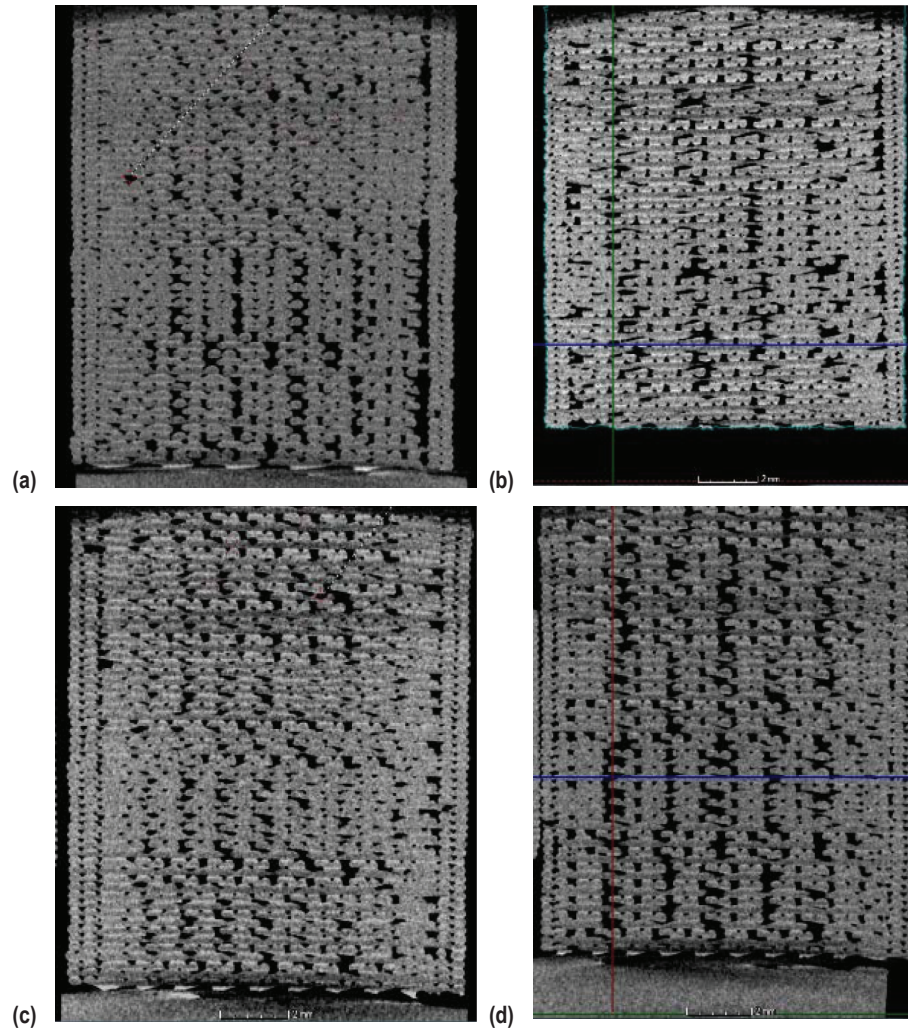
Figure 27. Computed tomography scans of compression specimens manufactured at various extruder standoff distances: (a) –0.02 mm extruder offset, (b) optimal condition, (c) 0.05 mm extruder offest, and (d) 0.1 mm extruder offset.

Misruns—adjacent layers cross over one another—were noted extensively for the compression specimens, indicative of limitations of the hardware in printing contours. A misrun is illustrated in figure 28.
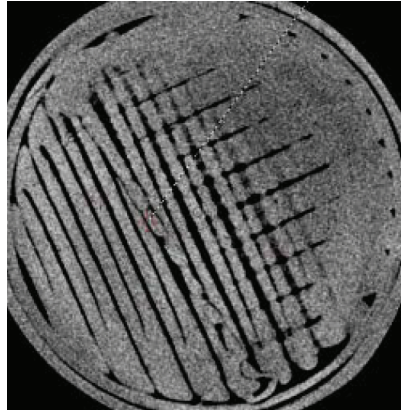
Figure 28. Illustration of misrun (overlap of adjacent layers) in specimen C4.
These are examples of printing errors observed throughout
the compression specimens at all process settings.

6.4.3 Layer Quality Specimens

Overall, there are no visually apparent substantive differences in material structure for the layer quality specimens, irrespective of the processing condition they were manufactured at. Representative cross sections of material in the x-z plane are shown for each manufacturing setting in figure 29. Voids are characteristic throughout the specimens, but there is not a clear visual trend in size, frequency, and distribution of voids with extruder standoff distance.
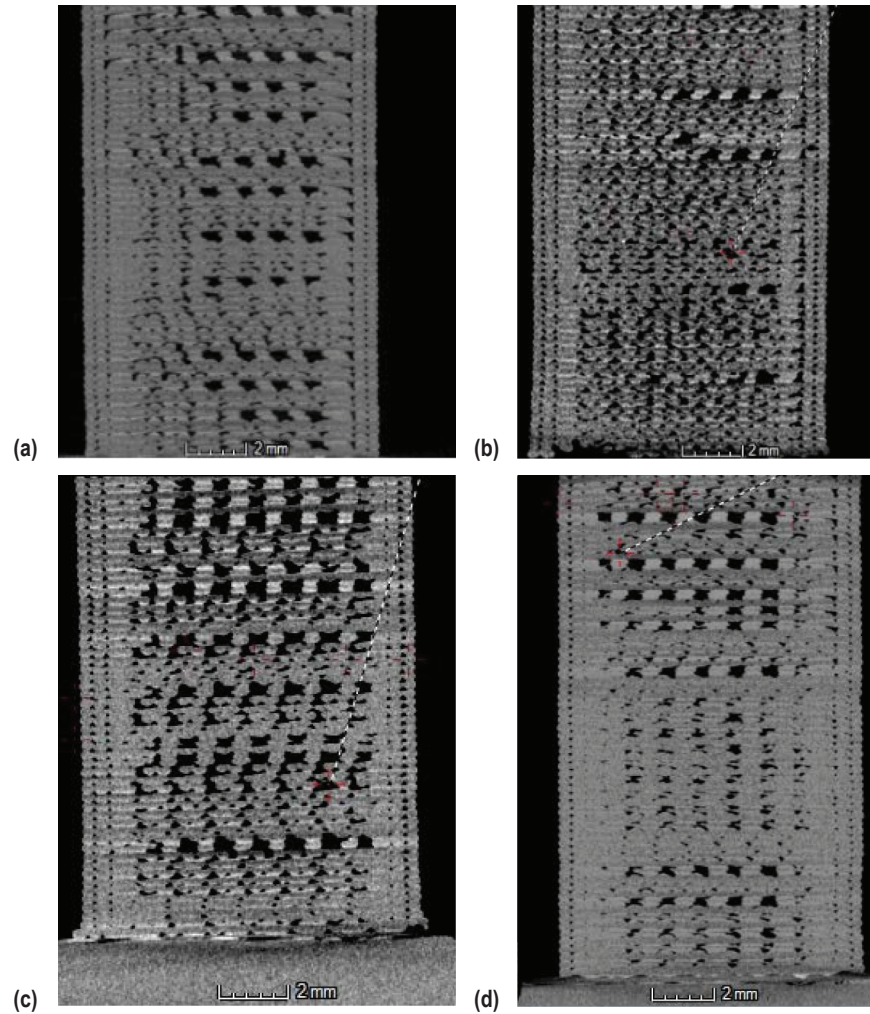
Figure 29. Computed tomography scans of layer quality specimens manufactured at various extruder standoff distances: (a) –0.02 mm extruder offset, (b) optimal condition, (c) 0.05 mm extruder offset, and (d) 0.1 mm extruder offset.

None of the features discussed in this section were classified as defects since it is not clear what, if any, impact these features have on mechanical performance. Further controlled studies would be required to determine the extent to which the size and frequency of voids, the presence of inclusions, and incidents of misrun degrade material strength.

7. SURFACE METROLOGY

7.1 Key Findings

Surface metrology was performed on four compression cylinders from the extruder stand-off distance study—one at each manufacturing process setting. The purpose of this testing was to provide a more detailed assessment of the 'out of round' behavior noted during structured light scanning of the flight compression specimens from phase I operations and determine whether the increased eccentricity noted for the flight compression specimens in the x-y plane could be attributed to variations in the process settings between the ground and flight prints. Ultimately, variability of compression test results observed in phase I may be partially attributable to these geometric differences. The surface metrology analysis of specimens from the extruder standoff distance study also served as a demonstration of surface metrology laboratory capabilities for future in-space manufacturing specimens. Both surface metrology and structured light scanning techniques represent efficient methods to assess the impact of dimensional variation and geometric differences on mechanical performance. Specific measurements and analyses are detailed below.

Ultimately, surface metrology data cannot definitively validate the hypothesis that increased out of round behavior noted in the flight compression specimens—which would be analogous to the 0.1 mm manufacturing process setting in this study—resulted in their weaker performance. The analysis does confirm that increased deviations from nominal geometry are more pronounced for off-nominal manufacturing process settings, but ultimately, the link between geometric variation and mechanical performance cannot be well characterized from the limited data set.

The number of samples at each manufacturing process condition makes it difficult to draw conclusions about relationships between parameters measured in surface metrology and manufacturing process condition. The content here is intended more as a demonstration of a capability that may be used for further in-space manufacturing studies. The analyses are incredibly detailed and only one specimen was analyzed at each setting to expedite the acquisition of data and enable a cursory assessment in a reasonable time frame. For the purposes of this study, the analysis is considered ancillary to other 'core' analysis techniques for in-space manufacturing, but future specimen sets may be enhanced by the targeted surface metrology analyses demonstrated here.

7.2 Results and Discussion

Conventional contact dimensional metrology was used to measure the following parameters for the four cylinders analyzed: diameter, length, and cylindrical form. Cylindrical form includes an assessment of roundness and eccentricity, 2D axial profile straightness and parallelism, and top face (x-y plane) flatness and squareness.

7.2.1 Diameter

Diameter was measured using a similar contact methodology for pin gauging—two point contact between spherical contact probes of a 1.6 mm radius with 0.14 N (14 g) gauge force. Diameter measurements were taken in six locations: three locations along the length, near the ends, and in the middle, and two locations around the circumference 90 degrees apart. The six diameter locations minimally encapsulate the diameters of the cylinder for size and provide for minimal insight to the form—barrel shape, hour glass, taper, straightness, out of roundness, etc.—that will be more thoroughly assessed via a high-resolution roundness and cylindricity measurement. A summary of the diameter measurements is given in table 9. The maximum diameter, minimum diameter, average diameter over six locations, and range of measurement are tabulated.

Table 9. Summary of diameter measurements (mm) for compression cylinders.

	−0.02 mm D	Nominal	0.05 mm	0.10 mm
Maximum diameter	12.72	12.7	12.72	12.79
Minimum diameter	12.31	12.31	12.24	12.24
Average diameter	12.49	12.52	12.49	12.55
Diameter range	0.41	0.39	0.48	0.55

Because of the small sample size (only four samples were analyzed and only one at each manufacturing process setting), it is difficult to discern trends in the diameter data. The diameter range over the six measurement locations does seem to slightly increase at a closer standoff distance, which may be suggestive of the more eccentric geometry observed for the flight specimens—also built with the extruder too close to the build plate—in phase I.

7.2.2 Length

The height of the specimens was measured with an electronic height gauge and surface plate. The height gauge uses a spherical contact probe of 2.5 mm radius applied with a 1 N gauging force. The average length and the parallelism are assessed from length measurements between the surface plate and five discrete locations on the specimen's top surface.

Length results for the specimens are summarized in table 10, which contains the maximum length measurement, minimum length measurement, average length measurement, and range of measurements for all measurement locations. The range of lengths is essentially the parallelism of the axial faces over a 10 mm diameter circle.

Table 10. Summary of length measurements (mm).

	−0.02 mm	Optimal	0.05 mm	0.10 mm
Maximum length	25.49	25.4	25.32	25.12
Minimum length	25.41	25.37	25.28	25.11
Average length	25.44	25.38	25.29	25.11
Range of lengths	0.09	0.03	0.03	0.01

Sample size makes it difficult to draw clear conclusions about the relationship between extruder standoff distance and resulting part geometry, but the cylinder does 'shrink' slightly in length as standoff distance decreases. Cylinders produced at the 0.1 mm condition may, be in a prestressed state, which could lead to a reduction in mechanical performance relative to the other specimens. This is one potential explanation for the reduced mechanical strength observed in the phase I flight data set, where compression specimens built at the closer extruder standoff distance were weaker than their ground counterparts.

7.2.3 Cylindricity

The cylindricity was assessed with a dedicated stylus-type roundness and cylindricity instrument (fig. 30). For roundness profile measurements, the cylinder rotates with the table and the gauge stylus is stationary. Measurements can be made at multiple axial locations to define a cylinder and cylindrical datum axis from the sample. Measurements assess the localized roundness, axial profile, and end face flatness. From these measurements, a variety of related dimensional and form attributes were assessed. Figure 31 shows a cylinder map of the compression cylinder manufactured at optimal process settings. The color map corresponds to eccentricity of the specimen from the cylindrical (best fit) datum.
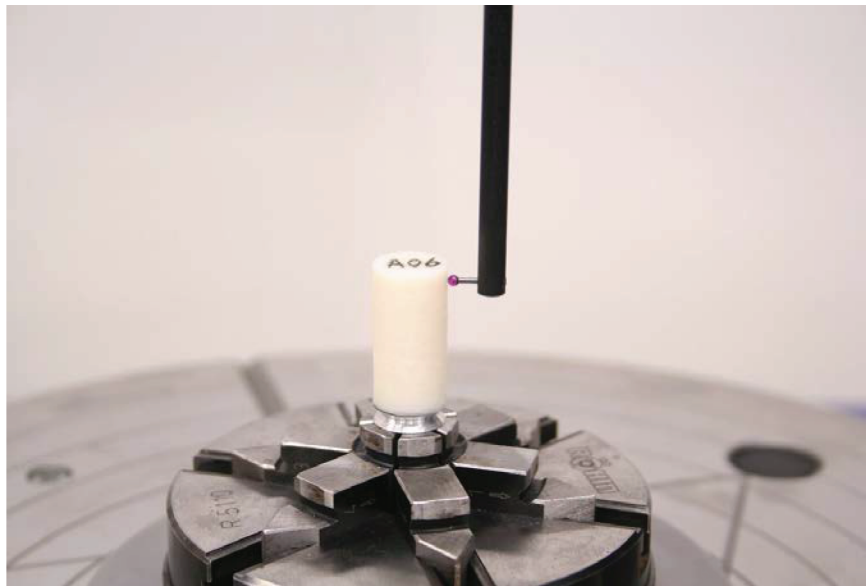
Figure 30. Cylindricity measurement of compression cylinder.
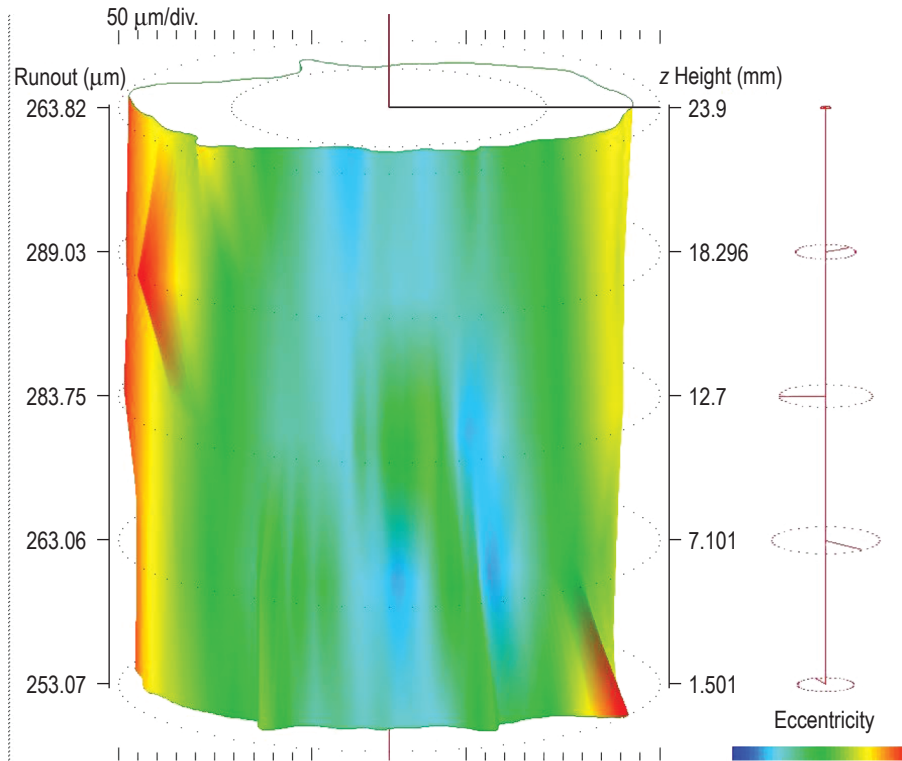
Figure 31. Cylinder mapping of cylinder manufactured at nominal processing condition.

Characteristic cylindricity measurements (defined here as the radial separation of two co-axial cylinders fitted to the total surface, such that their radial difference is at a minimum) are summarized in table 11. Cylindricity can be considered a metric to assess the tolerance of a part along its length. A tighter tolerance—reduced dimensional variation from the best-fit cylinder along the length of the part—corresponds to a smaller cylindricity value.

Table 11. Summary of cylindricity measurements.

	−0.02 mm	Optimal	0.05 mm	0.1 mm
Cylindricity (μm)	329	293	349	363

Based on the measurements in this dataset, off-nominal conditions for the extruder tip biased in either direction result in an increase in cylindricity. The greatest radial separation is observed for the 0.1 mm setting.

7.2.4 Roundness and Eccentricity

Roundness and eccentricity results are summarized in table 12. Measurements were taken at mid length at five locations clocked circumferentially. Roundness measures how closely the shape of the cylinder at a specific location along its axial length (here $z = H/2$) approaches that of a circle (fig. 32). Larger measurements correspond to more out-of-round geometries. Eccentricity also measures deviation from a perfect circle, but is a vector quantity that has both magnitude and direction. All measurements show some degree of variability with location, but the variation in the direction of eccentricity with clocking is significant. No consistent trends in roundness and eccentricity data measured only at mid length—across specimens are noted.

Table 12. Average roundness and eccentricity measurements at mid length.

	−0.02 mm D	Optimal A	0.05 mm C	0.1 mm B
Average roundness (μm)	277.4	271	290	274.8
Range of roundness measurement	101	33	49	52
Standard deviation	41.3	14.7	18	21.3
Average eccentricity magnitude (μm)	12.8	3.6	5	8.8
Range of eccentricity measurement	17	5	6	14
Standard deviation	6.8	1.9	2.8	5
Average eccentricity direction (deg)	122.8	135.6	206.4	137.2
Range of eccentricity direction	223	289	202	242
Standard deviation of eccentricity direction	105.5	121	94.5	101.3

Scale 0.2 mm/div.

90°

180°   0°

Reference Point
R –44956.80 μm
Theta 0°

Current Point
R 52.23 μm
Theta 45°

270°

Difference
Delta R 45009.03 μ
Delta Theta 45°
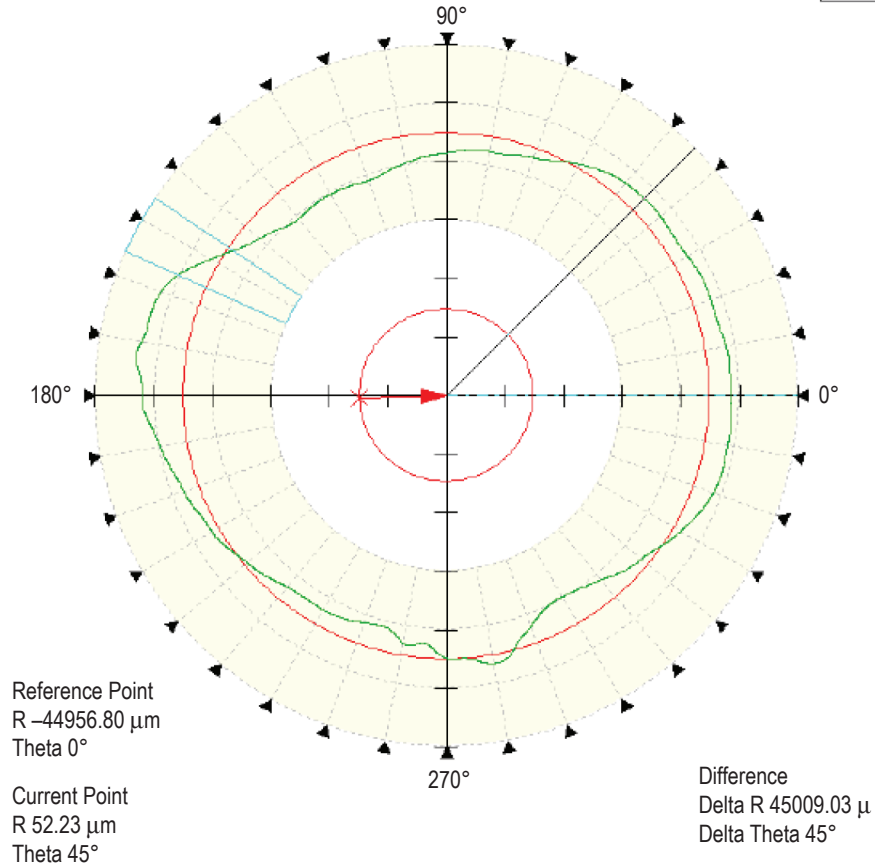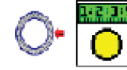
Figure 32. Roundness and eccentricity measurements at mid length for cylindrical
specimen manufactured at optimal condition.

Axial straightness along the specimen length was additionally measured as part of the cylinder mapping (fig. 33). Profile traces along the length of the specimen were taken at four locations (0, 90, 180, and 270 degrees). The axial straightness measurements are summarized in table 13. Values represent deviation of the outer geometry from the central (straight line) axis of the part.
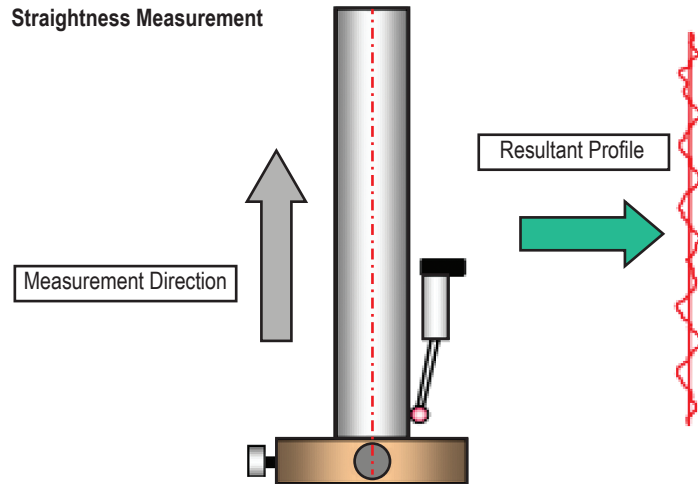
Figure 33. Diagram illustrating straightness measurement and resultant profile.

Table 13. Summary of axial straightness measurements with clocking
for each specimen.

	−0.02 mm	Optimal	0.05 mm	0.1 mm
000	102	89	153	467
090	142	150	167	484
180	317	89	274	414
270	393	144	478	244

Skewness results from the ends of the specimens, which exhibit some protrusions that create inflated deviations from the straight line fit. The axial straightness data with these end effects removed (by truncating data from 1 mm of the trace on either end of the specimen) appears in table 14. No clear and consistent trends in the data with the manufacturing process setting are evident.

Table 14. Summary of skewness measurements with clocking
for each specimen.

	−0.02 mm	Optimal	0.05 mm	0.1 mm
000	94	89	63	118
090	142	150	128	125
180	95	103	128	130
270	110	147	184	115

The flatness of the face, calculated based on five concentric circular traces of the sample (fig. 34) with 1.5 mm separation, was also measured (table 15). Off-nominal processing conditions may create a rougher surface, although the 0.1 mm condition, where the extruder tip is moved 0.1 mm closer to the part from its nominal position, has a roughness that is similar to the optimal specimen. More data would be needed to assess the impact of extruder standoff distance on flatness. The flatness measurements are of less immediate relevance to the extruder standoff distance study, but were undertaken as a demonstration of a measurement capability that may be desired for future in-space manufacturing analysis activities related to electronics substrate manufacturing.
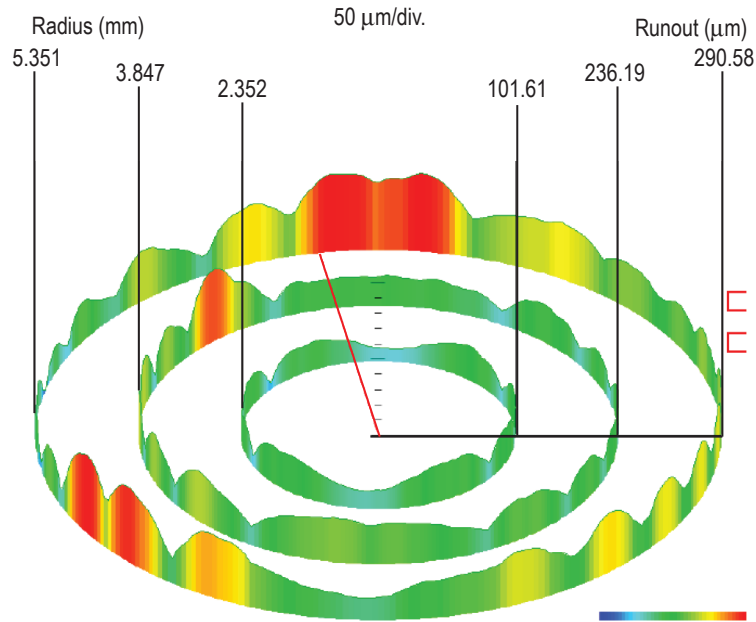
Figure 34. Flatness measurement of compression cylinder made at optimal manufacturing settings.

Table 15. Summary of flatness measurements.

	−0.02 mm	Optimal	0.05 mm	0.1 mm
Flatness (μm)	348.62	256.55	334.87	285.26

Compression cylinders were also measured via scanning laser confocal microscopy for 3D axial profile and to analyze more localized surface topography. The lateral sides of the compression cylinders are formed by the stacking of individual build layers. The edges of these layers protrude from a nominal boundary to yield distinct sharp valleys and rounded peaks when viewed in profile along the build (z) direction. Profiles were extracted from a surface topography along the middle of each cylinder that include about eight to nine build layers. For each layer, layer height (from valley to valley), the height of the layer 'bump' or protrusion (mean valley to peak), the area under the profile from valley mean line to peak, and the peak radius were measured. A full-length profile was also extracted from a longer topography.

None of these metrics showed much variation with manufacturing process settings. Build layer heights (fig. 35) are consistent across conditions, as are protruded heights of layers (fig. 36).
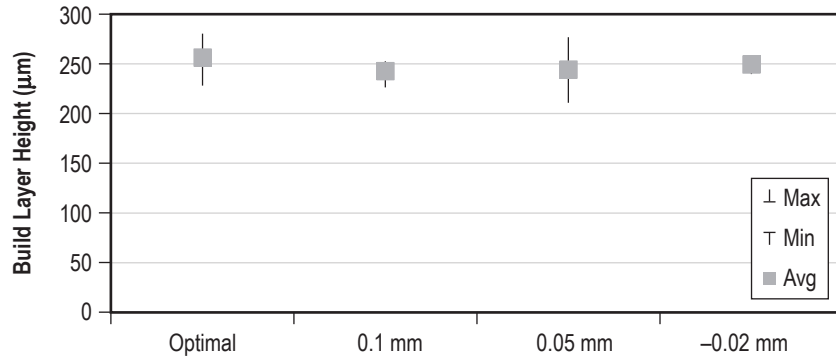
Figure 35. Build layer height across manufacturing process settings
for compression cylinders analyzed.
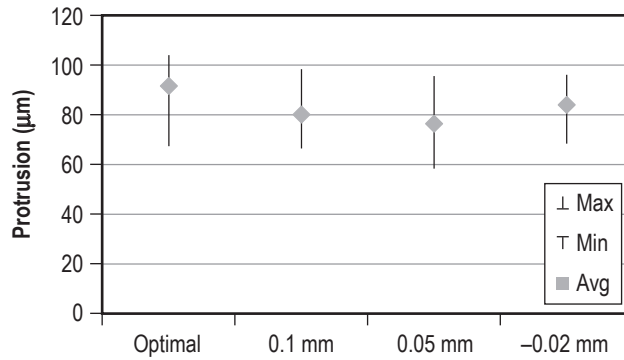
Figure 36. Build layer lateral protrusion across manufacturing process settings
for compression cylinders analyzed.

Further analysis of data investigated correlations between surface metrology data with compressive strength data (table 16). The aspect ratio of the cylindrical specimens (length divided by diameter) calculated from the metrology measurements was evaluated against mechanical performance data (ultimate compressive strength). From the metrology data, variations in length and diameter were the only clearly discernable relationships across manufacturing conditions. There is not a strong correlation here between extruder standoff distance, aspect ratio, and UTS. However, the aspect ratio does decrease slightly as the extruder moves closer to the build tray. Cylinders with a smaller aspect ratio should be able to resist higher loads, but this is contraindicative to the flight specimens for phase I, where the closer extruder tip to build plate distance—which presumably decreases the aspect ratio of the resulting specimen—resulted in a comparatively weaker part to the ground specimens. However, there may be interactive, competing effects, such as eccentricity of the part and the presence and distribution of voids, which make it exceedingly difficult to explain the phase I compression data in terms of extruder standoff distance alone.

Table 16. Extruder standoff distance, part geometry, and mechanical performance.

Extruder Setting	Aspect Ratio	Cylindricity	Ultimate Compressive Strength (ksi)
–0.02 mm	2.04	329	6.17
Optimal	2.03	293	5.74
0.05 mm	2.02	349	6.06
0.1 mm	2	363	6.11

8. SCANNING ELECTRON MICROSCOPY ANALYSIS

8.1 Key Findings

Tensile fracture surfaces at each level of print head offset were evaluated using SEM. Tensile comparisons within the same series show a correlation with the fracture surfaces. The high strength samples appear to be denser and the lower strength samples consistently have a less dense open structure. In the less dense structures, the fibers appear to not be strongly bonded to the surrounding fibers, potentially resulting in slippage during the tensile test. There are differences in the builds within a specimen class despite being made at the same manufacturing process setting. Overall microscopy suggests a large degree of build to build variability for the 3DP hardware. Clear and consistent trends in the variation of material structure with extruder standoff distance were not noted, with the exception of the fiber protrusions at the base of the specimen at the 0.05 mm and 0.1 mm extruder standoff conditions.

The compression samples produced at each print head offset were also evaluated with microscopy. Optical images were taken of the top and edge surfaces of the tested compression cylinders. Backscatter electron (BSE) images were taken of the top and edge surfaces to compare to the optical images. After initial analysis, the samples were cross sectioned and polished. BSE images were taken of the cross sections to show any internal defects such as voids.

The compression specimens did not reveal a clear and consistent trend in outer appearance or internal structure with the manufacturing process settings considered in this study. Optically, each sample set is similar. Each specimen, regardless of manufacturing condition, contains surface defects along the sides. These indications are suggestive of printing defects where the fiber is distorted. Each cross section showed voids in the center of the sample. Some variations were observed on the top faces of the samples. On some specimens, the fibers appear to have contact with the fibers on either side throughout the entire surface. On other specimens, there was some separation between the fibers on the surface, possibly due to variations in printing. (These misruns and print errors were also noted in CT.) As with CT, the compression analysis detailed here fails to shed further light on the disparate compression properties between the flight and ground prints noted in phase I specimen analysis.

8.2 Results and Discussion

8.2.1 Tensile Specimens

8.2.1.1 Series A: Optimum. For the three tensile samples manufactured at the optimal print head setting, A3 had a significantly higher tensile strength (fig. 37). Looking across the optical images, the fracture surface of A3 is much different than A1 or A2. As seen in figure 38, the internal structure of A3 appears to be denser (highlighted in green) than the structure of A1 or A2, where visible spaces (highlighted in red) can be observed between the fibers. It is likely that the open structure of A1 and A2, as well as the apparent incomplete fusion of the layers, resulted in a lower tensile strength.
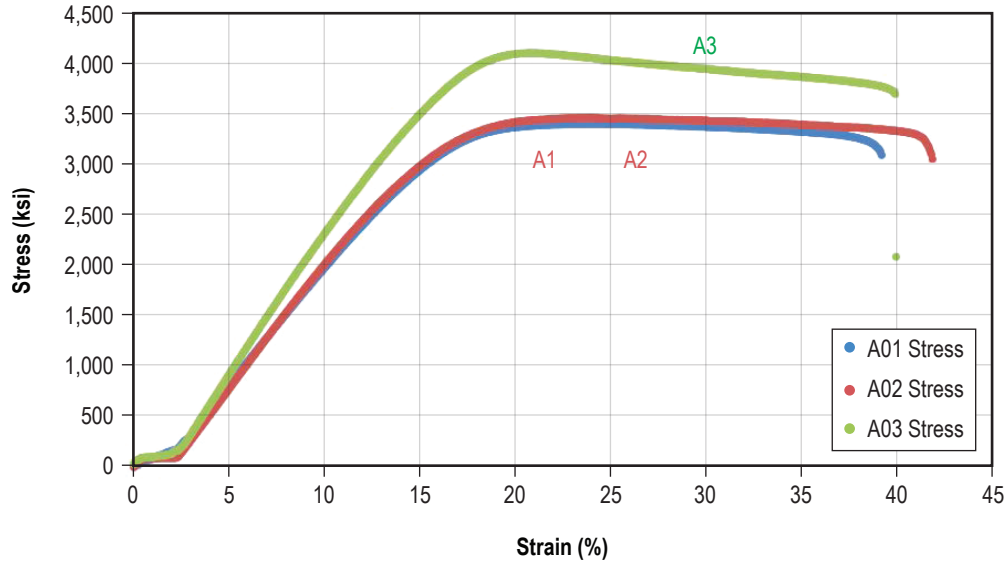
Figure 37. Tensile curves of specimens manufactured at optimal setting and corresponding optical microscope images. Regions of low and high density are highlighted in red and green, respectively.
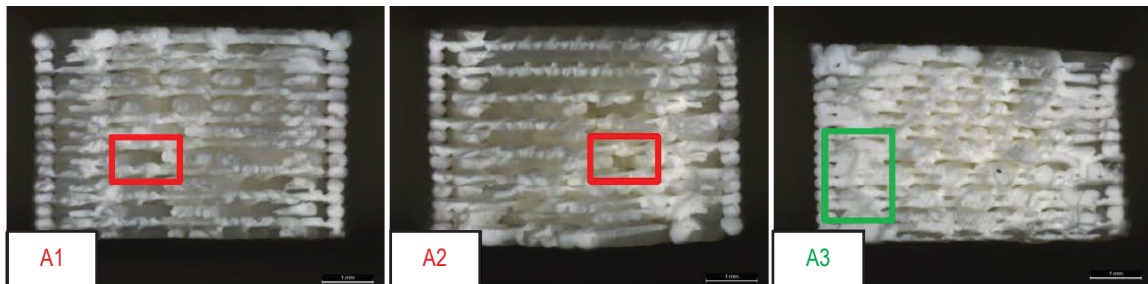

Figure 38. Cross sections of specimens manufactured at optimal print head setting. Regions of low and high density are highlighted in red and green, respectively.

8.2.1.2 Series B: 0.1 mm. The series B samples were made with the print head 0.1 mm closer to the sample plate relative to the optimal setting. Figure 39 shows two of B samples had a higher tensile strength (B1 and B3). The optical images of these fracture surfaces show large areas where the plastic is dense (highlighted in green), likely contributing to its increased strength. However, there are also areas in these samples that have an open structure, where it appears there are no fibers or the fibers were loosely bonded and pulled away from the surrounding material (highlighted in red). Though B2 had a lower strength, there were areas that had a higher density, but the overall densification was not as great as in specimens B1 and B3. Figure 40 summarizes the observations from the B series.

Figure 39. Tensile curves of specimens manufactured at the 0.1 mm offset condition and corresponding optical microscope images. Regions of low and high density are highlighted in red and green, respectively.

Figure 40. Cross sections of specimens manufactured at the 0.1 mm print head setting. Regions of low and high density are highlighted in red and green, respectively.

8.2.1.3 Series C: 0.05 mm. The series C samples were made with the crosshead 0.05 mm closer to the sample plate than at the optimal manufacturing condition. Each of these samples had approximately the same strength (fig. 41). C2 was slightly higher performing. The optical images show that C2 may be slightly denser than C1 or C3, although all the samples have some localized regions of high density. Materials from the C specimen class have a mostly open structure relative to previously examined specimen classes (fig. 42).
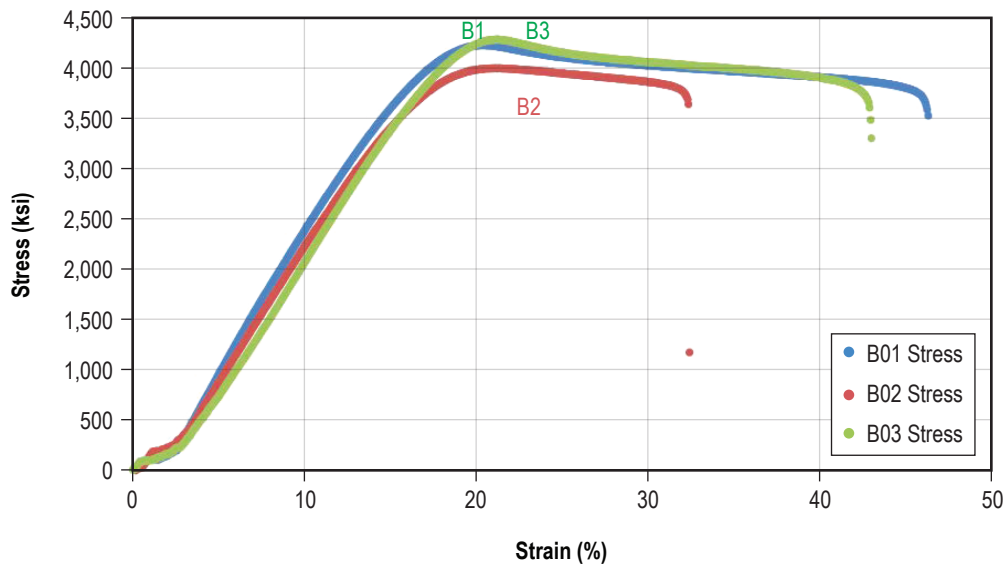

Figure 41. Tensile curves of specimens manufactured at the 0.05 mm offset condition and corresponding optical microscope images. Regions of low and high density are highlighted in red and green, respectively.

Figure 42. Cross sections of specimens manufactured at the 0.1 mm print head setting. Regions of low and high density are highlighted in red and green, respectively.

8.2.1.4 Series D: –0.02 mm. The series D samples were made with the crosshead –0.02 mm from the nominal position. The tensile data show that samples D2 and D3 have a much higher strength than that of D1 (fig. 43). The optical images of D2 and D3 show large areas that are highly dense (highlighted in green), though there are also areas with a more open structure where it appears the fibers did not bond to one another tightly (highlighted in red). To contrast, the lower strength D1 sample has a mostly open structure where a lack of fiber bonding is readily apparent (fig. 44).
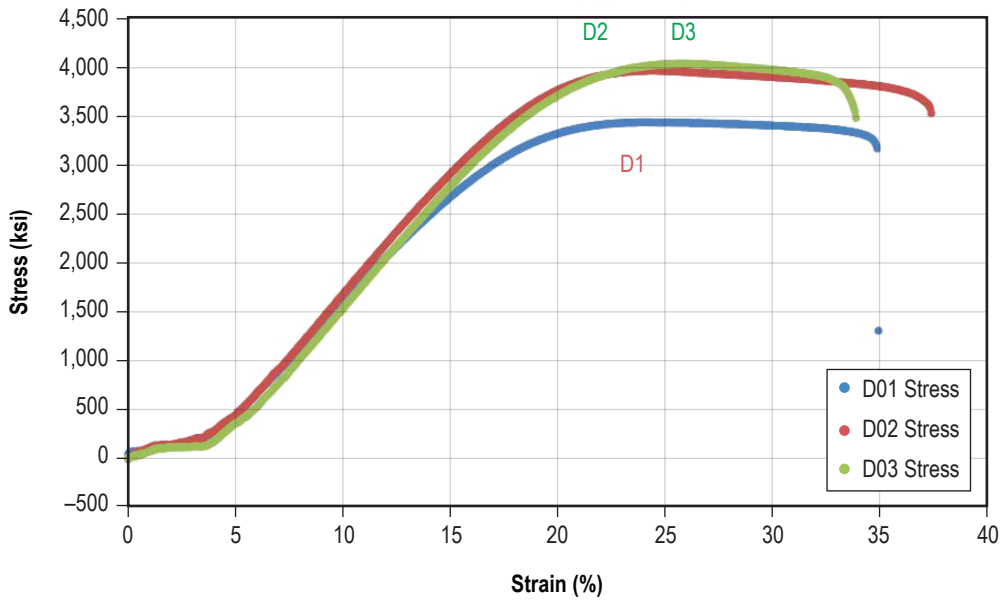
Figure 43. Tensile curves of specimens manufactured at the –0.02 mm offset condition and corresponding optical microscope images. Regions of low and high density are highlighted in red and green, respectively.
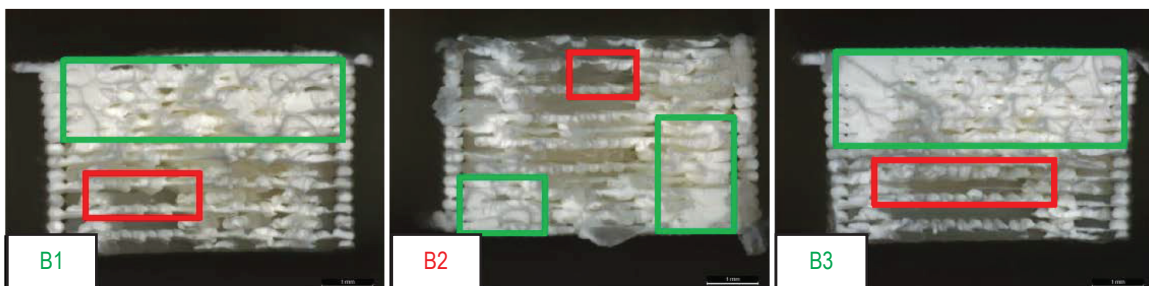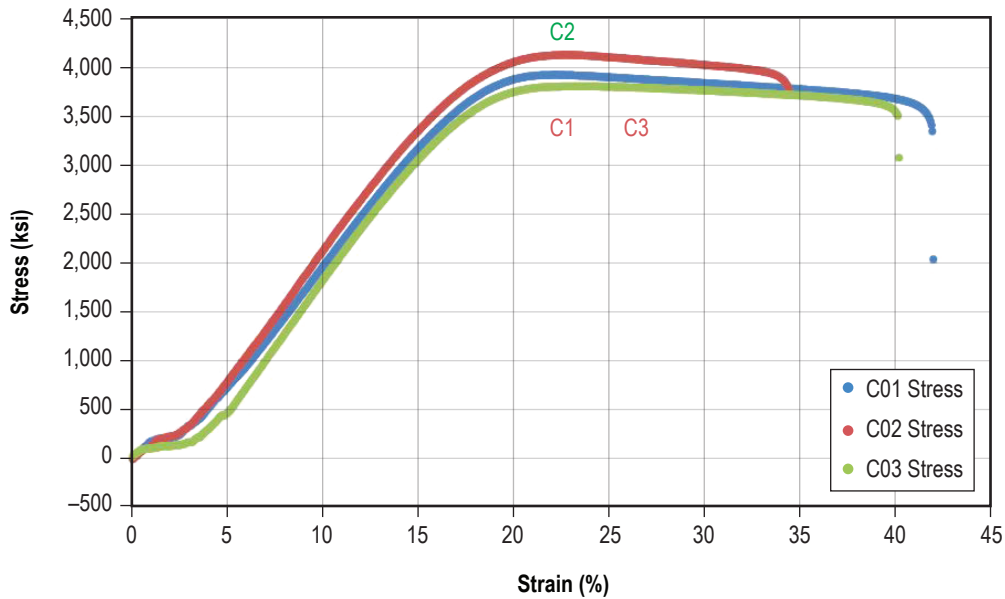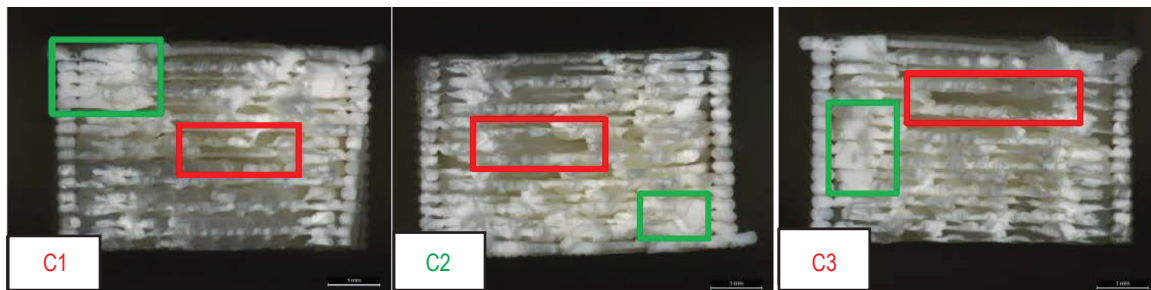

Figure 44. Cross sections of specimens manufactured at the –0.02 mm print head setting. Regions of low and high density are highlighted in red and green, respectively.

8.2.2 Compression Specimens

For the compression specimens at each manufacturing process setting, optical images were taken of the top and edge surfaces. BSE images were taken of the top and edge surfaces to compare with the optical images. After initial optical microscopy analysis, the samples were cross sectioned and polished. BSE images were also taken of the cross sections.

8.2.2.1 Series A: Optimum. In figure 45, rows (a) and (b) compare the optical and BSE images, respectively, of the top surface of the compression specimens. The surfaces appear fairly consistent between manufacturing settings, although A04 and A05 show some separation between the fibers (indicated by the red boxes). Rows (c)–(e) compare the optical ((c) and (d)) and BSE (row (e)) of the side surface. The reflected X shapes on each sample are imperfections. The BSE images show these imperfections in closer detail. They appear to be printing defects where the fiber is distorted and could indicate a print error (also observed in the CT scans). Row (f) is a BSE image of the cross section showing voids within each sample. These appear to be a separation between the fiber layers where the sample is not fully dense.

Figure 45. Rows (a) and (b) compare the BSE images of the top surface of the compression specimens manufactured at the optimal setting. Rows (c) and (d) compare the optical images of the side surface. Row (e) is the BSE image of the side surfaces. Row (f) contains BSE images of the cross sections.

8.2.2.2 Series B: 0.1 mm. In figure 46, rows (a) and (b) compare the optical (row (a)) and BSE (row (b)) images of the top surface. The surfaces of B4 and B5 are relatively free of voids, originating from separation between fibers, although the B6 surface exhibits more significant separation (highlighted in red).

Rows (c)–(e) compare the optical (rows (c) and (d)) and BSE images (row (e)) of the side surfaces for the specimens manufactured at the 0.1 mm extruder setting. Reflected X shapes on the optical samples are imperfections. The BSE images show close-up images of the imperfections. As with series A (optimal manufacturing condition), these imperfections appear to be a result of printing defects. Row (f) is a BSE image of the cross section. Voids (separation between the fiber layers where the sample is not fully dense) are evident.
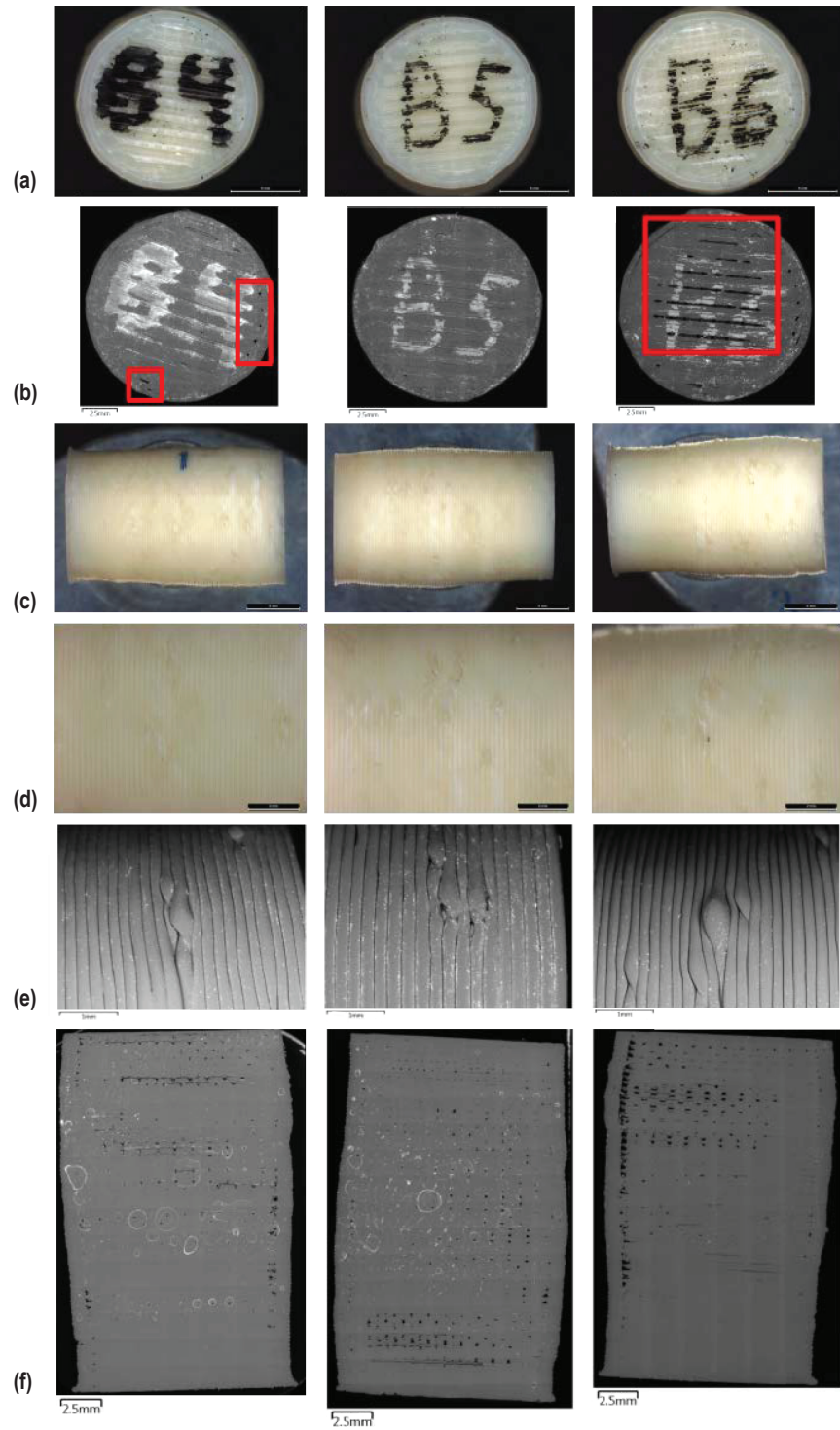
Figure 46. Comparison of compression specimens at the 0.1 mm extruder setting. Row (a) is optical images of the top surfaces. Row (b) is BSE images. Rows (c) and (d) are optical images of the side surfaces. BSE images of the side surfaces are in row (e). Row (f) shows BSE images of the specimen cross sections.

8.2.2.3 Series C: 0.05 mm. Series C is shown in figure 47. As with the other specimen sets, rows (a) and (b) compare the optical (row (a)) and BSE (row (b)) images of the top surface. All three samples are relatively free of voids (separation between fibers). Rows (c)–(e) compare the optical (rows (c) and (d)) and BSE (row (e)) of the side surface. On each sample, imperfections are shown on the optical samples as a reflected X shapes. The BSE images show these imperfections at higher magnification, which appear to be printing defects where the fiber is distorted. Row (f) is a BSE image of the cross section, showing voids within each sample. Separations between the fiber layers where the sample is not fully dense are evident.

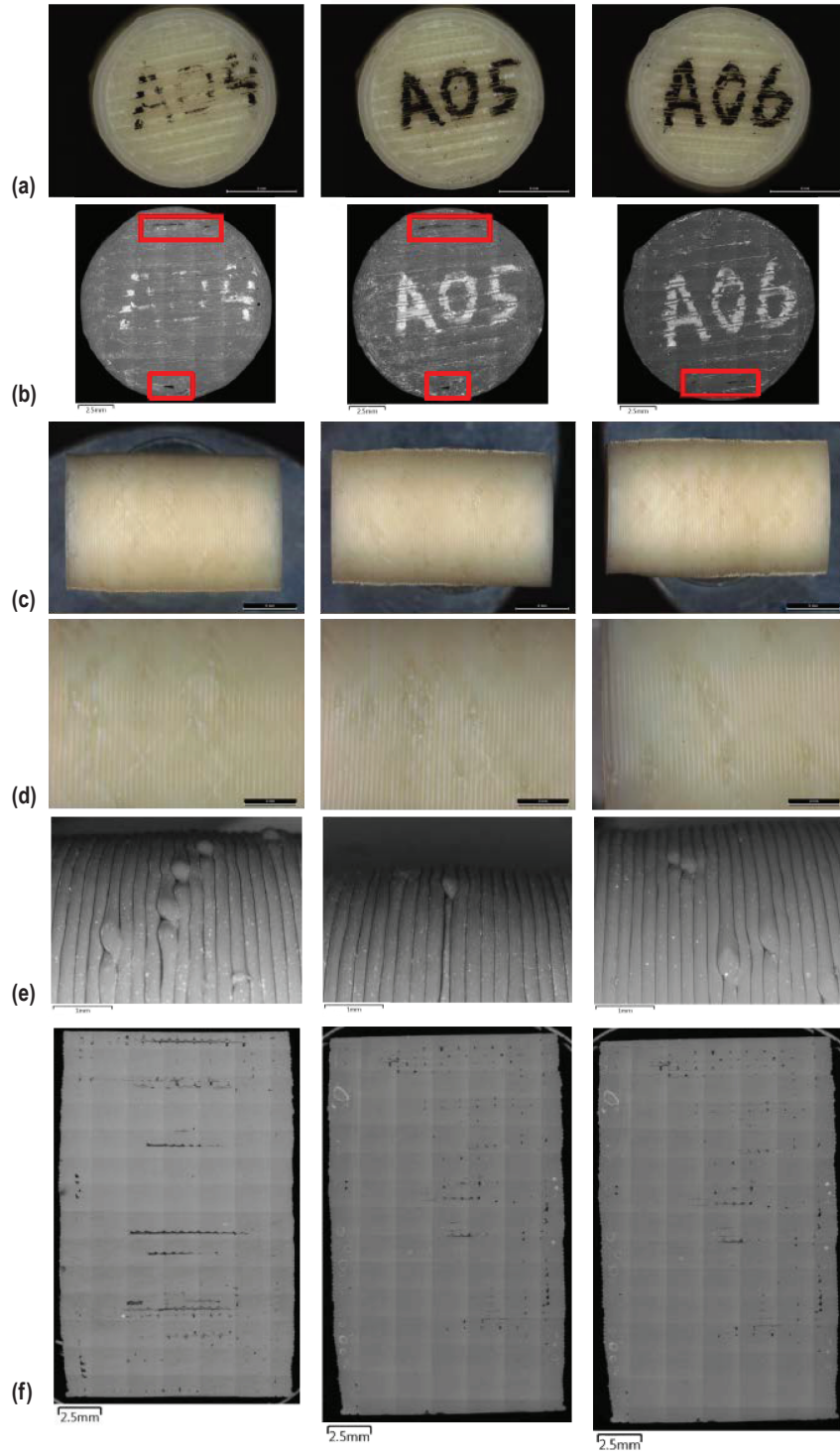Figure 47. Row (a) contains optical images of the top surfaces of the C-class (0.05 mm extruder setting) specimens. Row (b) shows the corresponding BSE images of the top surfaces. Row (c) and (d) are optical images of the side surfaces. Row (e) shows BSE images of the side surfaces. Row (f) shows BSE images of the specimen cross sections for C4, C5, and C6, respectively.

8.2.2.4 Series D: –0.02 mm. Microscope images of the series D specimens (manufactured at the –0.02 mm extruder condition) are shown in figure 48. Rows (a) and (b) compare the optical (row (a)) and BSE (row (b)) images of the top surfaces for D4, D5, and D6. While all the surfaces of each sample have voids (separation between the fibers), D5 is much denser than D4 or D6 (highlighted in red).

Rows (c)–(e) compare the optical (rows (c) and (d)) and BSE (row (e)) of the side surface. On each sample, imperfections are indicated on the optical samples as reflected X shapes. The BSE images in row (e) show these imperfections at a higher magnification. Mirroring the findings of CT, these appear to be printing defects where the fiber is distorted. Row (f) is a BSE image of the cross section, showing voids within each sample. Voids are the separation between the fiber layers where the sample is not fully dense.
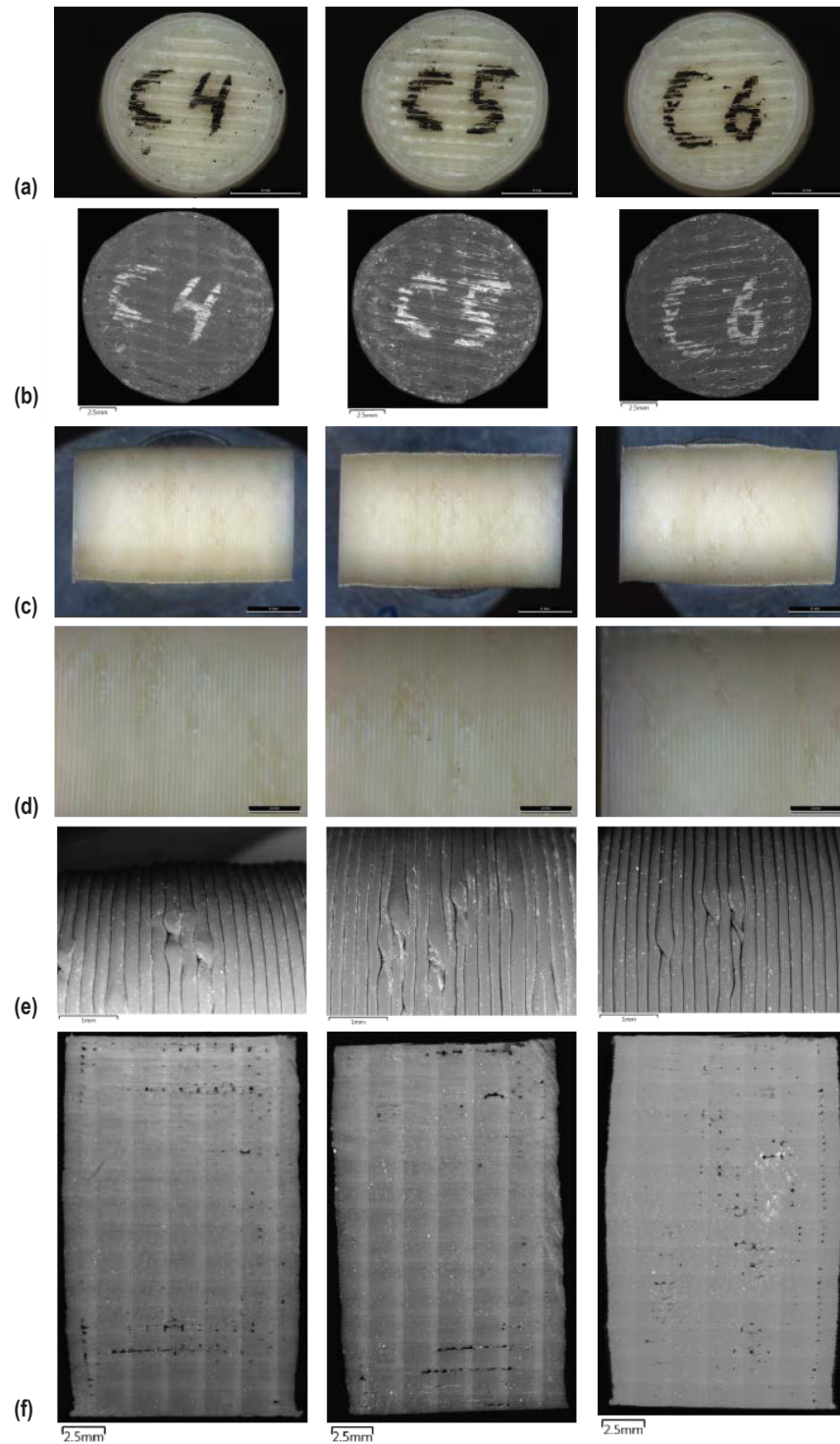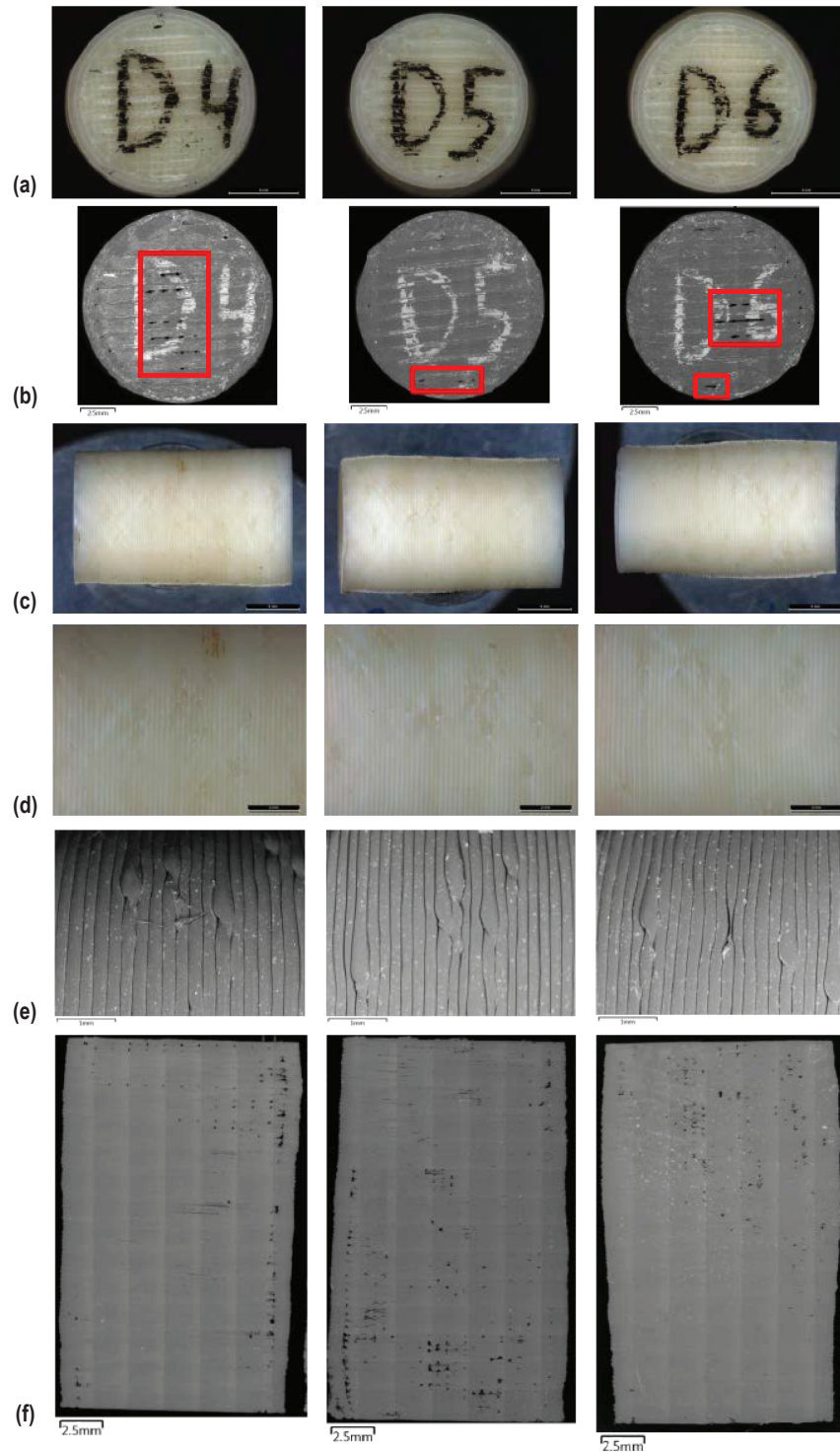
Figure 48. Row (a) contains optical images of the top surfaces of the D-class (–0.02 mm extruder setting) specimens. Row (b) shows the corresponding BSE images of the top surfaces. Row (c) and (d) are optical images of the side surfaces. Row (e) shows BSE images of the side surfaces. Row (f) shows BSE images of the specimen cross sections for D4, D5, and D6, respectively.

9. SUMMARY OF THE EXTRUDER STANDOFF DISTANCE STUDY AND CONCLUSIONS

In the extruder standoff distance study, ABS samples were manufactured with the goal of observing variations in material outcomes with differences in the print head offset (z-height). Four series of samples were printed: optimum, 0.1 mm (extruder tip 0.1 mm closer to the build plate than its nominal condition), 0.05 mm, and –0.02 mm (extruder tip –0.02 mm farther away from the build plate than its nominal condition). The window of movement of the extruder tip was defined by a previous screening study to determine how close or far away the extruder tip could be moved from an optimal position across all specimen geometries while still yielding a viable print that could be tested. Variations at the extremes of the experimental matrix (–0.02, the farthest position of the extruder tip from the build tray and 0.1 mm, the closest position of the extruder tip to the build tray) approximate the manufacturing process settings for the ground and flight prints from 3DP phase I, respectively, which exhibited substantial differences in material structure and mechanical performance.

The primary objective of the study is to quantify the influence of the distance between the extruder tip and the build plate during specimen manufacture on density, mechanical performance, internal material structure, and dimensional variation and determine whether relationships observed can be extrapolated to potentially explain variations noted between ground and flight prints from phase I.

The study seeks to assess whether extruder standoff distance can be considered the primary source of variability in the phase I data set. Analysis of phase I specimens ultimately suggested that the variation in manufacturing process settings during operation of the printer, particularly during flight prints where the extruder standoff distance was adjusted during the course of operations based on visual feedback, offered the most viable explanation for material discrepancies between flight and ground specimens. Subsequent chemical analyses were not suggestive of a material aging effect or moisture absorption and SEM evaluation of flight and ground specimens showed large structural differences that were suggestive of operational changes in the manufacturing process.[3] This exercise in manufacturing process optimization with the ETU also serves to inform subsequent operation of the 3DP unit on the ISS should it occur, as well as development of requirements for future space-based manufacturing capabilities.

Key findings from the study include the following:

• Total mass of extrudate is not dependent on extruder standoff distance.

• A clear and consistent relationship between density and extruder standoff distance is not observed. For the compression specimens, the closest setting (0.1 mm) is in family with the lower density flight prints.

- Overall, UTS and elastic modulus improve as the specimens are built closer to the extruder tip. This finding mimics the phase I results, where flight specimens built with the extruder closer to the build tray exhibited slightly enhanced mechanical performance relative to the ground prints.

- A clear relationship between extruder standoff distance and material performance in compression was not detected by these experiments. The stronger mechanical behavior noted for the ground prints (built at a greater standoff distance) and comparatively weaker behavior of the flight prints (built at a smaller standoff distance) is not replicated in this data set. Ground compression specimens from phase I of the 3D printing in zero G tech demo are distinct from any other specimen set/manufacturing processing condition considered in this study. Flight compression specimens are in family with the 0.1 mm processing condition, but they are also in family with all other specimen sets in the extruder standoff distance study.

- SEM analysis, structured light scanning, and CT show protrusions at the base of the tensile specimens made at the closer extruder standoff distances that contribute to an artificial strengthening of the part. These features could enhance mechanical performance relative to specimens built farther away from the extruder tip that do not possess reinforcing structural features which align with the load path during tensile testing.

- Based on structured light scanning results, extruder standoff distance has a strong impact on form and geometry of the resultant specimen. Tensile specimens seem to be more susceptible to geometric variations resulting from differences in processing conditions.

- No consistent relationship in bulk density and extruder standoff distance for compression and layer quality specimens was detected based on quantitative CT data. Clear trending is apparent in the tensile specimens, as mean CT (and the bulk density calculated based on this value) of the tensile coupon increases as the extruder tip moves closer to the build tray.

- Computed tomography examination of compression specimens and layer quality specimens does not show a strong relationship between internal material structure and the extruder distance setting, although the larger 'gaps' between layers of material noted for the 0.1 mm compression specimen are a structural feature that could contribute to premature failure relative to other specimens with less spacing. Compression specimens at the 0.1 mm setting—closest position of the extruder tip to the build tray considered—were, on average, the weakest specimens.

- Surface metrology analysis, while performed on only a small subset of specimens, suggests that increased deviations from nominal geometry are more pronounced for off-nominal manufacturing process settings. This corroborates findings of structured light scanning. The greatest cylindricity (dimensional variation from the 'best fit' cylinder along the length of the part) is observed for the 0.1 mm specimen (closest distance of extruder tip to build plate).

- From SEM, lower strength samples consistently have a less dense open structure (observed for ground tensile specimens from phase I). There are significant structural differences in the builds across a given manufacturing processing condition—the layer spacing may be different for each sample in the series, despite being made at the same process setting. Microscopy data suggest a significant degree of build-to-build variability for the 3DP hardware in terms of internal material structure.

Results of the study suggest that discrepancies in tensile performance between flight and ground prints can likely be explained by differences in manufacturing process settings, specifically the reduced extruder standoff distance for the flight prints, which resulted in protrusions at the base of the specimen that contribute to enhanced mechanical strength—a phenomenon which is to some extent replicated here. An explanation for differences in compression specimen structure and performance for 3DP phase I ground and flight groups cannot be readily extrapolated from this study, but key findings from CT, structured light scanning, and surface metrology suggest that decreasing extruder standoff distance results in specimens with increased dimensional variation (cylindricity), shrinkage, and air gaps in the through-thickness. There is a significant degree of variability between builds at any single process setting in terms of material structure and mechanical performance. It is, thus, possible that the build-to-build variability may overwhelm other potential sources of variation in the data set, making it difficult to isolate variables and pinpoint the degree to which changes in a specific manufacturing process variable are linked to differences in material outcomes. Cooling rate is a key determiner of microstructure and material performance. Inherent limitations of the hardware, specifically the uncontrolled thermal environment, also impeded a rigorous assessment of the impact of manufacturing variables.

Results presented herein have a high specificity to the ETU, as this was a focused study designed only to answer open questions related to the 3DP phase I data set from the 3D printing in zero G technology demonstration mission. The limited window of process variation was selected to broadly mimic manufacturing operational differences between phase I flight and ground prints of the 3D printing in the zero G technology demonstration. The results of this study serve as further illustration that characterization of the printer cannot be separated from characterization of the material. Material outcomes are closely linked to the machine and manufacturing process settings used to produce the specimens. All analyses detailed in this TP indicate significant build-to-build variability for the hardware. This variability is substantial enough to potentially explain differences in the ground and flight prints independent of manufacturing processing conditions. The material discrepancies noted in phase I were likely a combination of differences in manufacturing process settings, build-to-build variability, and print errors. There are no analyses to date that point to operation of the FDM process in microgravity as a substantive, engineering significant, contributing factor to material differences. The high degree of build-to-build variability for additive manufacturing (AM) hardware makes it difficult to develop optimal process operating windows by linking processing parameters to material outcomes. This variability is recognized as a key challenge across the entire AM industry and applies to almost all hardware and processes. Methods to apply controls and adjustments for machine variability is a near-term focus area for AM.[8]

The 3D printing in zero G technology demonstration mission was highly successful and exceeded the performance baselines set for the mission. Mission accomplishments to date include: printing of 21 parts from phase I, printing of 34 parts from phase II (currently being tested), demonstration of the ability to uplink a file from the ground and print it on-orbit, manufacture of functional tools that could be used in the space environment, and successful operation of hardware and a manufacturing capability that could transform current logistics paradigms for human spaceflight. Made in Space, Inc. leveraged lessons learned from the 3DP technology demonstration mission to develop a commercial facility for the Space Station, the Additive Manufacturing Facility, which has a heated bed, enhanced control and automation, can print with multiple material feedstocks, and is used by multiple customers, including NASA.

Testing of specimens from the second phase of operations of the 3D printing in the zero G technology demonstration mission is underway. For this phase of operations, which took place in June and July 2016, the *z*-calibration was set via a calibration print and held constant over the course of the next 24 prints. For the final 9 specimens in the 34-specimen print matrix, the extruder standoff distance was decreased from the optimal condition by 0.1 mm, mimicking both the phase I flight prints and the B series prints from the study summarized here. Tensile, compression, and layer quality specimens were produced at both manufacturing process settings during phase II flight operations. Subsequent analysis of this data set, currently underway, will be the most informative in assessing differences in ground processed versus flight processed material.

APPENDIX

Tables 17–21 give specimen masses; summaries of tensile specimen, compression specimen, and layer quality specimen density values; and the average densities across specimen sets, respectively.

Table 17. Specimen masses.

Specimen Type	Average Mass (g)	Coefficient of Variation (%)
–0.02 mm, tensile	4.97	0.6
Optimal. tensile	5.01	0.5
0.05 mm, tensile	5.02	0.7
0.1 mm, tensile	4.98	0.6
Ground tensile	5.02	0.2
Flight tensile	4.98	1.2
–0.02 mm, compression	2.88	2.1
Optimal, compression	2.89	0.9
0.05 mm, compression	2.88	1.1
0.1 mm, compression	2.82	1.5
Ground compression	2.93	1.7
Flight compression	2.81	1
–0.02 mm, layer quality	2.68	1.6
Optimal, layer quality	2.69	0.7
0.05 mm, layer quality	2.66	2.1
0.1 mm, layer quality	2.67	2
Ground layer quality	2.61*	N/A*
Flight layer quality	2.65*	N/A*

* Only one layer quality specimen was produced at ground and flight conditions for 3DP phase I. Average in ground and flight entry represents a single data point and thus has no variability associated with it.

Table 18. Summary of tensile specimen density values.

Manufacturing Processing Condition	Average Density (g/cc)	Coefficient of Variation (%)
–0.02 mm	0.93	2.5
Optimal	0.92	1.5
0.05 mm	0.94	3
0.1 mm	0.96	1.5
Ground	0.9	0.9
Flight	0.93	2.2

Table 19. Summary of compression specimen density values.

Manufacturing Processing Condition	Average Density (g/cc)	Coefficient of Variation (%)
–0.02 mm	0.94	1.6
Optimal	0.94	0.1
0.05 mm	0.95	0.2
0.1 mm	0.91	1.3
Ground	0.94	1.5
Flight	0.91	1

Table 20. Summary of layer quality specimen density values.

Manufacturing Processing Condition	Average Density (g/cc)	Coefficient of Variation (%)
–0.02 mm	0.93	1.3
Optimal	0.93	1.7
0.05 mm	0.92	1.7
0.1 mm	0.93	1.5
Ground	0.89*	N/A*
Flight	0.92*	N/A*

* Only one layer quality specimen was produced at ground and flight conditions for 3DP phase I. Average in ground and flight entry represents a single data point and thus has no variability associated with it.

Table 21. Average densities across specimen sets (specimens grouped by manufacturing processing condition).

Manufacturing Processing Condition	Average Density (g/cc)	Coefficient of Variation (%)
–0.02 mm	0.93	1.6
Optimal	0.93	1.3
0.05 mm	0.94	2.1
0.1 mm	0.94	2.5
Ground	0.92	2.4
Flight	0.92	1.3

Plots of tensile specimens produced at –0.02 mm, optimal, 0.05 mm, and 0.1 mm calibration conditions are given in figures 49–52, respectively. Figures 53–56 show a comparison of compression curves for specimens produced at the –0.02 mm, optimal, 0.05 mm, and 0.1 mm calibration setting, respectively.
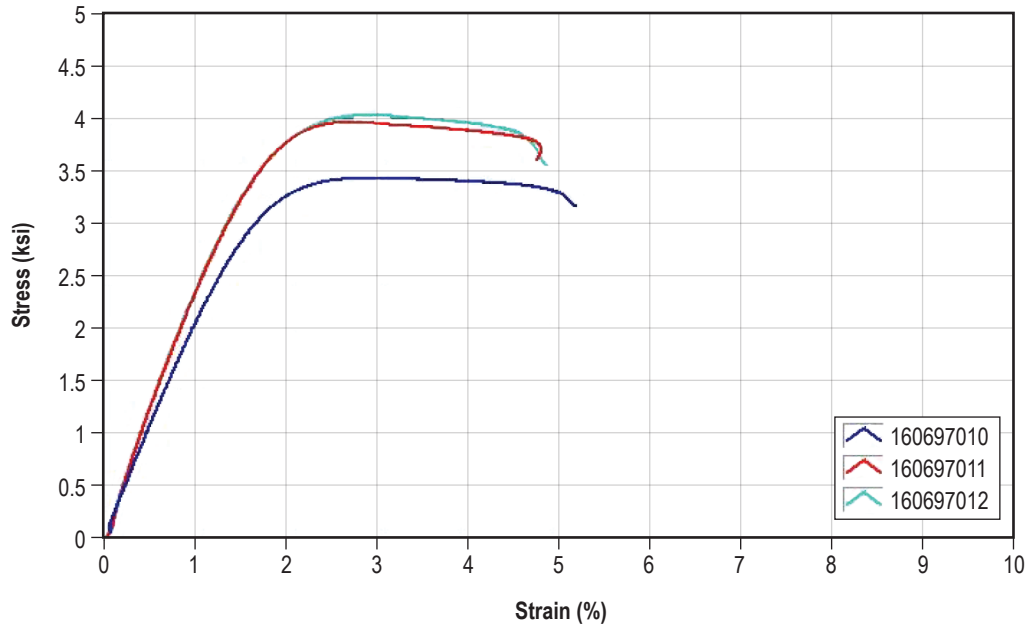
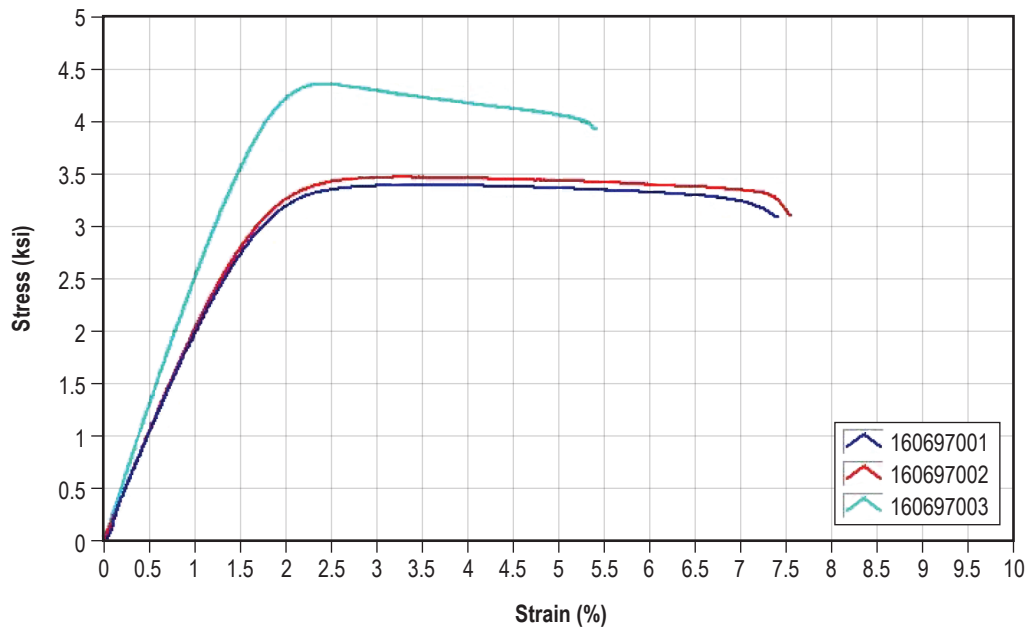Figure 49. Plot of tensile specimens produced at –0.02 mm calibration condition.

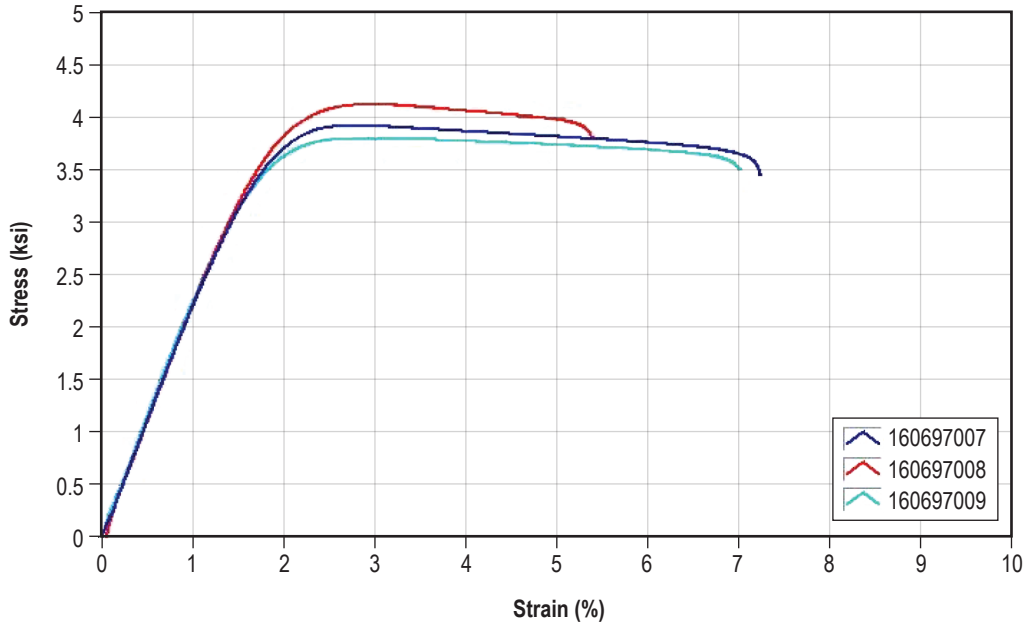Figure 50. Plot of tensile specimens produced at optimal calibration condition.

Figure 51. Plot of specimens produced at 0.05 mm calibration condition.
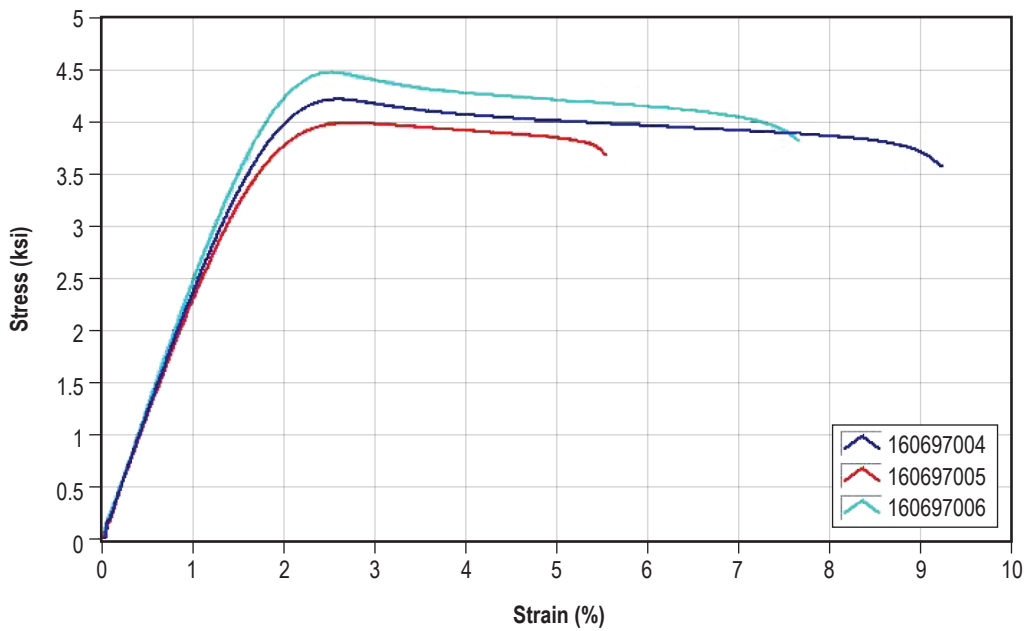

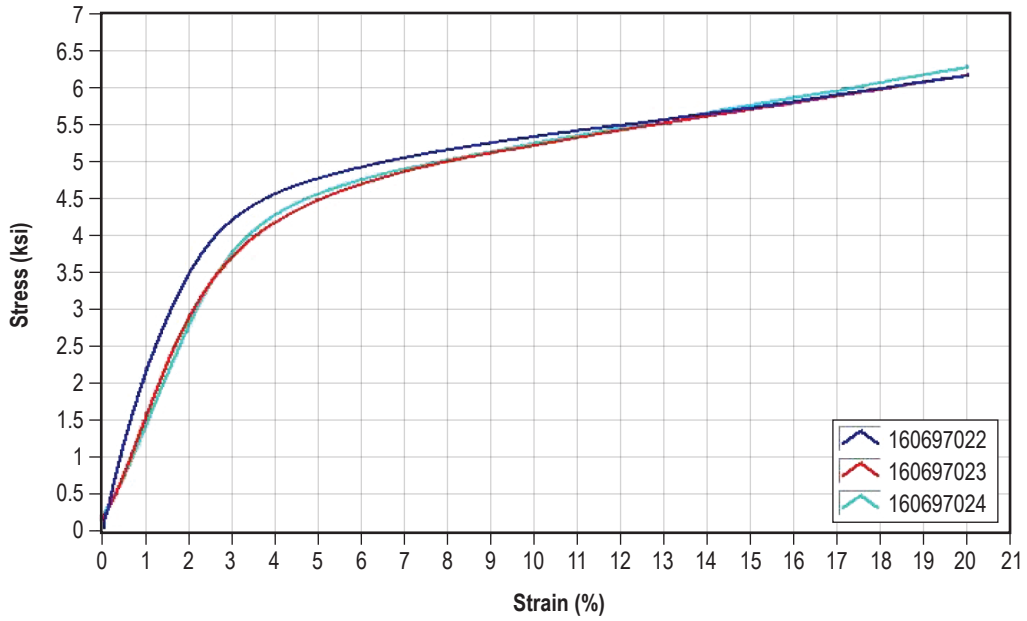Figure 52. Plot of tensile specimens produced at 0.1 mm calibration condition.

Figure 53. Comparison of compression curves for specimens produced
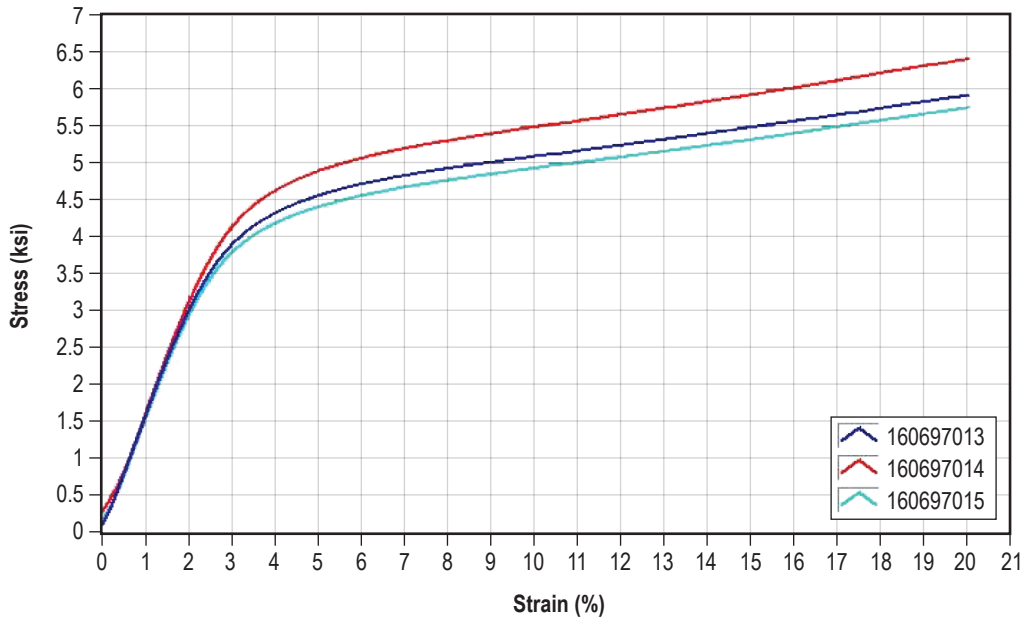at the –0.02 mm calibration setting.

Figure 54. Comparison of compression curves for specimens produced
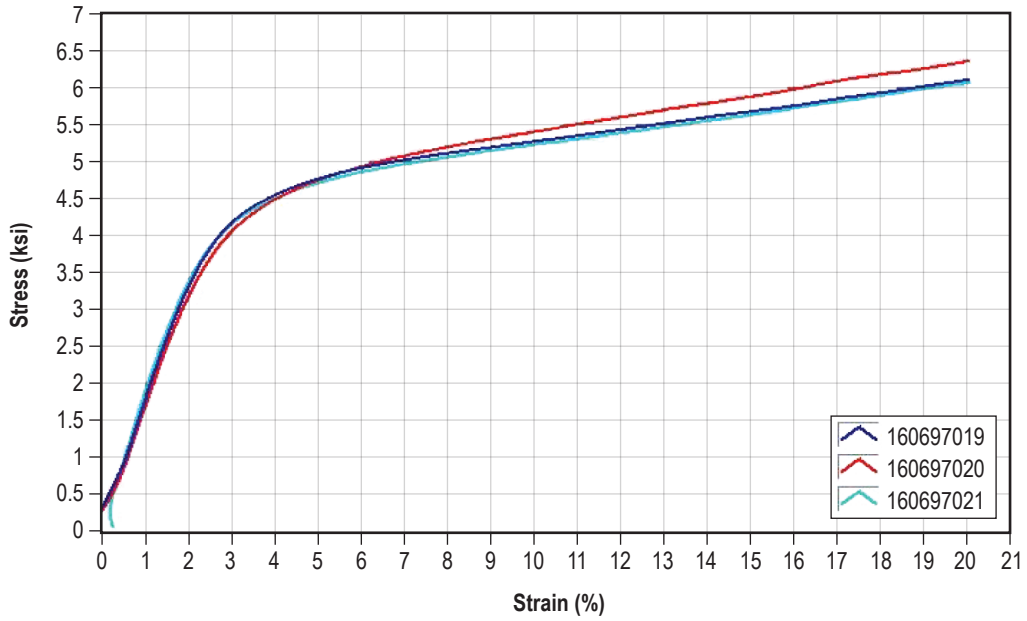at the optimal calibration setting.

Figure 55. Comparison of compression curves for specimens produced
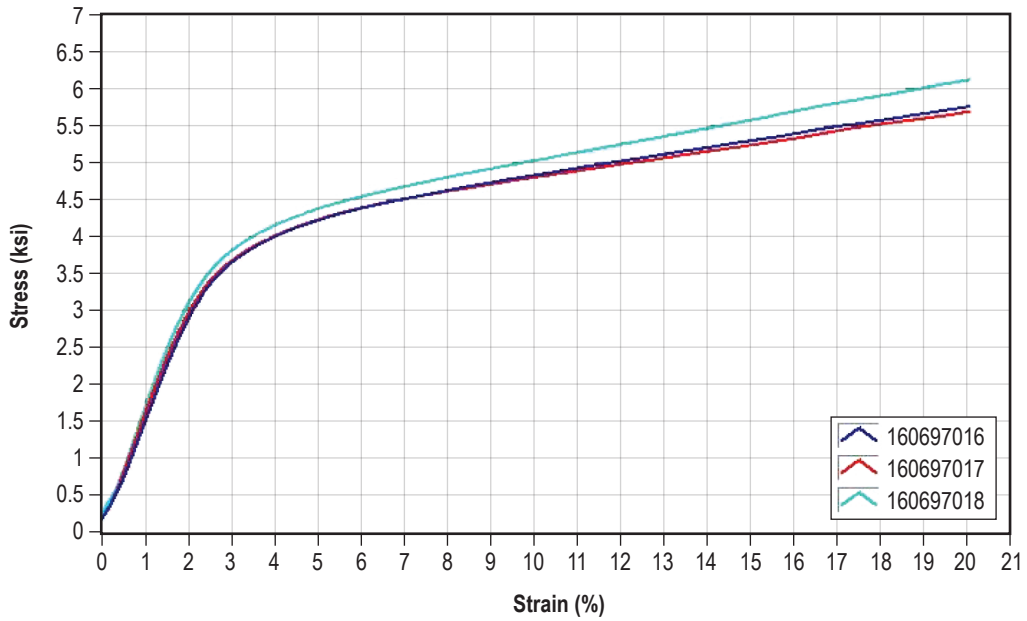at the 0.05 mm calibration setting.

Figure 56. Comparison of compression curves for specimens produced
at the too close calibration setting (0.1 mm).

Following is the procedure for the calculation of relative density compared to ABS from the CT data:

(1) A region of interest in the CT volume image of the specimen is selected. The region is defined such that it captures the maximum possible volume within the specimen without including surrounding air or supporting material.

(2) VGStudio's volume analyzer tool measures the mean CT number of the selected volume in the specimen and reports the mean value.

(3) A region of interest in the CT volume image of the solid ABS reference disk is selected. Region is defined such that the volume selected is contained within the ABS disk without including the volume of the test specimen, supporting structures, or inherent artifacts in the outer perimeter of the CT image. Mean value of CT is recorded.

(4) Calculate the ratio of the mean CT number of the specimen volume to the mean CT number of the solid ABS reference disk. This ratio may be used to estimate the physical density of the specimen by multiplying the ratio with the known physical density of the ABS reference disk.

(5) Visual review of each CT slice. Record images of any identified anomalies. If many similar anomalies appear in a specimen, provide a representative image and note the presence of such anomalies in terms of location in the specimen; i.e., throughout specimen, near center, upper region of scanned volume, etc.

(6) Repeat steps (1) through (5) for each specimen.

REFERENCES

1. Owens, A.C.; and DeWeck, O.: "Systems Analysis of In-Space Manufacturing Applications for International Space Station in Support of the Evolvable Mars Campaign," *Proceedings of AIAA SPACE 2016*, AIAA 2016-5034, <http://dx.doi.org/10.2514/6.2016-5394>, 2016.

2. Prater, T.J.; Bean, Q.A.; Werkheiser, N.; et al.: "Summary Report on Results of the 3D Printing in Zero G Technology Demonstration Mission, Volume 1," NASA/TP—2016–219101, NASA Technical Reports Server, <http://ntrs.nasa.gov/search.jsp?R=20160008972>, NASA Marshall Space Flight Center, Huntsville, AL, 2016.

3. Prater, T.J.; Bean, Q.A.; Werkheiser, N.; et al.: "Analysis of specimens from phase I of the 3D Printing in Zero G Technology demonstration mission," *Rapid Prototyping Journal*, accepted for publication, 2017.

4. Rodriguez, J.F.; Thomas, J.P.; and Renaud, J.: "Characterization of the mesostructure of fused deposition acrylonitrile-butadiene-styrene materials," *Rapid Prototyping Journal,* Vol. 6, pp. 175–186, 2000.

5. ASTM D638, "Standard Test Method for Tensile Properties of Plastics," ASTM International, West Conshohocken, PA, 2014.

6. ASTM D695, "Standard Test Methods for Compressive Properties of Rigid Plastics," ASTM International, West Conshohocken, PA, 2015.

7. Ziemian, C.W.; Sharma, M.M.; and Ziemian, S.N.; "Anisotropic Mechanical Properties of ABS Parts Fabricated by Fused Deposition Modelling," Dr. Murat Gokcek (Ed.), *Mechanical Engineering*, <http://www.intechopen.com/books/mechanical-engineering/anisotropic-mechanical-properties-of-abs-parts-fabricated-by-fused-deposition-modeling>, doi: 10.5772/34233, 2012.

8. Pellegrino, J.; Makila, T.; McQueen, S.; and Taylor, E.: "Measurement Science Roadmap for Polymer-Based Additive Manufacturing," *NIST Advanced Manufacturing Series 100-5,* <https://doi.org/10.6028/NIST.AMS.100-5>, December 2016.

REPORT DOCUMENTATION PAGE

1. REPORT DATE (DD-MM-YYYY) 01–06–2017	2. REPORT TYPE Technical Publication	3. DATES COVERED (From - To)

4. TITLE AND SUBTITLE

A Ground-Based Study on Extruder Standoff Distance for the 3D Printing in Zero Gravity Technology Demonstration Mission

5a. CONTRACT NUMBER

5b. GRANT NUMBER

5c. PROGRAM ELEMENT NUMBER

6. AUTHOR(S)

T.J. Prater Q.A. Bean, N.J. Werkheiser, R.D. Beshears, T.D. Rolin, E.M. Rabenberg, H.A. Soohoo, F.E. Ledbetter III,* and S.C. Bell**

5d. PROJECT NUMBER

5e. TASK NUMBER

5f. WORK UNIT NUMBER

7. PERFORMING ORGANIZATION NAME(S) AND ADDRESS(ES)

George C. Marshall Space Flight Center
Huntsville, AL 35812

8. PERFORMING ORGANIZATION REPORT NUMBER

M–1433

9. SPONSORING/MONITORING AGENCY NAME(S) AND ADDRESS(ES)

National Aeronautics and Space Administration
Washington, DC 20546–0001

10. SPONSORING/MONITOR'S ACRONYM(S)

NASA

11. SPONSORING/MONITORING REPORT NUMBER

NASA/TP—2017–219631

12. DISTRIBUTION/AVAILABILITY STATEMENT

Unclassified-Unlimited
Subject Category 27
Availability: NASA STI Information Desk (757–864–9658)

13. SUPPLEMENTARY NOTES

Prepared by the Materials & Processes Laboratory, Engineering Directorate
*Wheelhouse Consulting, LLC, Huntsville, AL **Jacobs Engineering, Huntsville, AL

14. ABSTRACT

Analysis of phase I specimens produced as part of the 3D printing in zero G technology demonstration mission exhibited some differences in structure and performance for specimens printed onboard the International Space Station (ISS) and specimens produced on the ground with the same printer prior to its launch. This study uses the engineering test unit for the printer, identical to the unit on ISS, to conduct a ground-based investigation of the impact of the distance between the extruder tip and the build tray on material outcomes. This standoff distance was not held constant for the phase I flight prints and is hypothesized to be a major source of the material variability observed in the phase I data set.

15. SUBJECT TERMS

additive manufacturing, fused deposition modeling, 3D printing in zero G technology demonstration mission, manufacturing process optimization, 3D printing, in-space manufacturing

16. SECURITY CLASSIFICATION OF:			17. LIMITATION OF ABSTRACT	18. NUMBER OF PAGES	19a. NAME OF RESPONSIBLE PERSON STI Help Desk at email: help@sti.nasa.gov
a. REPORT U	b. ABSTRACT U	c. THIS PAGE U	UU	94	19b. TELEPHONE NUMBER (Include area code) STI Help Desk at: 757–864–9658

National Aeronautics and
Space Administration
IS02
George C. Marshall Space Flight Center
Huntsville, Alabama 35812